WATER RESOURCES RESEARCH, VOL. ???, XXXX, DOI:10.1029/,

Zeroth-order inversion of transient head observations

D. W. Vasco

Berkeley Laboratory, University of California, Berkeley, California

(510-486-5206, e-mail:dwvasco@lbl.gov)

Berkeley Laboratory, University of California, Berkeley, California (e-mail:dwvasco@lbl.gov)

Abstract. A high frequency, asymptotic solution for transient head, appropriate for a medium containing smoothly-varying heterogeneity, provides a basis for efficient inverse modeling. The semi-analytic solution is trajectory-based, akin to ray methods used in modeling wave propagation, and may be constructed by post-processing the output of a numerical simulator. For high frequencies, the amplitude sensitivities, the relationship between changes in flow properties and changes in head amplitude, are dominated by the phase term which may be computed directly from the output of the simulator. Thus, transient head waveforms may be inverted with little more computation than is required to invert arrival times. An application to synthetic head values indicates that the technique can be used to improve the fit to waveforms. An application to transient head data from the Migration experiment in Switzerland reveals a narrow, high conductivity pathway within a 0.5 m thick zone of fracturing.

1. Introduction

In this paper I demonstrate how an iterative model updating scheme, can benefit from trajectory-based modeling. First, trajectory-based techniques provide efficient, semi-analytic expressions for solving the forward problem, for computing the residuals, and for computing the partial derivatives, the model parameter sensitivities. Secondly, trajectory-based methods provide additional flexibility in formulating the inverse problem. Specifically, in the trajectory-based approach the modeling is broken into two distinct steps: (1) the computation of a travel time, (2) the computation of the time-varying amplitude function. Thus, one can use travel times as a datum for characterization, an alternative to fitting the head observations directly. There is some advantage associated with the use of travel times. First, the inverse problem associated with travel times is quasi-linear and thus convergence is less of an issue [*Cheng et al.*, 2005]. Furthermore, the inversion of travel times involves much less computation than does amplitude inversion. Thus, a useful strategy invokes an initial travel time inversion followed by an amplitude inversion. Trajectory-based modeling also provides, in the form of the trajectories, an easy way to visualize the relationship between observations and the region of the subsurface which influences the observations.

This paper compliments earlier work on trajectory-based modeling and inversion of transient head data [*Vasco et al.*, 2000; *Kulkarni et al.*, 2001; *Brauchler et al.*, 2003; *Vasco and Finsterle*, 2004; *He et al.*, 2006]. Here I provide efficient, approximate expressions for amplitude sensitivities which are alternatives to the more exact Born sensitivities given in *Vasco et al.* [2000]. The sensitivities, which are derived using a technique from high-

frequency seismic waveform inversion [*Vasco et al.*, 2003], are provided for all points on the transient head curve. The trajectory-based sensitivities require essentially the same level of computation as travel time sensitivities. However, the amplitude sensitivities allow one to invert transient head waveforms directly, avoiding the necessity of estimating arrival times. Using waveform data can be advantageous when interference effects, as due to multiple sources, make it difficult or impossible to identify a specific arrival from a particular source. Furthermore, inadequate time sampling may prevent one from estimating arrival times. In such a case one can still use the waveform observations to estimate flow properties, as shown in this paper.

2. Methodology

2.1. The Equation Governing Drawdown

In an inhomogeneous medium the equation describing the space $\mathbf{x}$ and time t evolution of head $h(\mathbf{x},t)$ is

$$K(\mathbf{x})\nabla^2 h(\mathbf{x},t) + \nabla K(\mathbf{x}) \cdot \nabla h(\mathbf{x},t) = S(\mathbf{x}) \frac{\partial h(\mathbf{x},t)}{\partial t} \tag{1}$$

where $K(\mathbf{x})$ denotes the hydraulic conductivity and $S(\mathbf{x})$ denotes the specific storage [*Bear*, 1972; *de Marsily*, 1986]. We consider the equation in the frequency domain, by applying the Fourier transform [*Bracewell*, 1978]

$$H(\mathbf{x},\omega) = \frac{1}{2\pi} \int_{-\infty}^{\infty} h(\mathbf{x},t) e^{i\omega t} d\omega \tag{2}$$

to equation (1). In the frequency domain equation (1) becomes

$$\nabla^2 H(\mathbf{x},\omega) + \mathbf{\Lambda}(\mathbf{x}) \cdot \nabla H(\mathbf{x},\omega) - i\omega\kappa(\mathbf{x}) H(\mathbf{x},\omega) = 0 \tag{3}$$

where I have divided through by $K(\mathbf{x})$ and defined

$$\mathbf{\Lambda}(\mathbf{x}) = \nabla \ln K(\mathbf{x}) \tag{4}$$

and

$$\kappa(\mathbf{x}) = \frac{S(\mathbf{x})}{K(\mathbf{x})}. \tag{5}$$

From equation (3) it is clear that for large ω, at high frequencies, the head is sensitive to $\kappa(\mathbf{x})$, the ratio of storage to conductivity. Conversely, low-frequency variations in head, such as a static change, are primarily sensitive to the spatial variation of $\ln K(\mathbf{x})$.

2.2. The Inverse Problem

Equation (3) comprises the forward problem in which one computes the observed head variations at an observation point, given the spatial distribution of hydraulic conductivity $K(\mathbf{x})$ and specific storage $S(\mathbf{x})$, a source function, and the boundary conditions. Solution of the forward problem, which requires the solution of the linear differential equation (1) or (3), is a stable procedure and results in unique values for $H(\mathbf{x}, \omega)$, given the appropriate initial data.

In the inverse problem one is given observations of head at a finite set of observation points and seeks estimates of both the head and the flow properties at all remaining points. Most of the difficulties encountered are related to the fact that there many fewer observations then there are model parameters. Thus, at most locations, the head and the flow properties are both unknown, and hence equation (3) contains product terms in pairs of unknowns, rendering it non-linear. Furthermore, because there are many fewer data than unknowns, one can encounter severe non-uniqueness, in which many, perhaps an infinite number, of models can explain the observations [*Parker*, 1994].

There are several ways to deal with the non-linearity and the non-uniqueness and thus provide solutions to the inverse problem. The most direct approaches range from simple trial and error to more sophisticated stochastic techniques. Most efficient methods are based in some fashion upon a local linearization about an initial or starting model which I shall denote by the vector $\mathbf{K}_0$. The idea is to derive a linear relationship between perturbations in the model, $\delta\mathbf{K}$, and perturbations in the data, $\delta\mathbf{H}$. For a finite dimensional model and a finite number of observations, I can write the linear relationship as a matrix equations

$$\delta\mathbf{H} = \mathbf{M}\delta\mathbf{K} \tag{6}$$

where $\mathbf{M}$ is the sensitivity matrix, the i-th, j-th entry is given by

$$M_{ij} = \frac{\partial H_i}{\partial K_j}. \tag{7}$$

I will give explicit examples of such linearizations below. The non-uniqueness is most frequently treated by attaching additional constraints on the desired model, in the form of penalty terms [*Parker*, 1994]. Penalty terms, such as the minimum norm and model roughness penalty, will be discussed in more detail below.

2.3. Asymptotic Solutions for Flow

An asymptotic solution for flow follows if I take a solution of the form

$$H(\mathbf{x},\omega) = e^{-\sqrt{i\omega}\sigma(\mathbf{x})}\sum_{n=0}^{\infty}\frac{A_n(\mathbf{x})}{(\sqrt{i\omega})^n} \tag{8}$$

[*Virieux et al.*, 1994]. The motivation for using an expansion in inverse powers of ω is that the initial terms of the series represent rapidly varying (high-frequency, large ω) components of the solution and successive terms are associated with lower frequency behavior [*Vasco and Datta-Gupta*, 1999]. The quantity σ, known as the 'phase' or 'pseudo-

phase', is analogous to the phase of a propagating wave [*Virieux et al.*, 1994]. In fact, as noted by *Vasco et al.* [2000], for an impulsive source, $\sigma(\mathbf{x})$ can be related to the arrival time of the peak of a head pulse. For a step function source $\sigma(\mathbf{x})$ is associated with the time at which the derivative of the head curve experiences a maximum, the arrival time of the peak slope at the point $\mathbf{x}$. Thus,

$$\sigma(\mathbf{x}) = \sqrt{6 T_{peak}(\mathbf{x})} \tag{9}$$

where $T_{peak}(\mathbf{x}_s)$ is the arrival time of the peak at the observation point $\mathbf{x}$ [*Virieux et al.*, 1994; *Vasco et al.*, 2000]. The functions $A_n(\mathbf{x})$, in equation (8), provide successive corrections to the head amplitude. The reason for using $\sqrt{i\omega}$ in the series, rather than simply ω, is that I would like the solution to reduce to the expression for head in a homogeneous medium [*Virieux et al.*, 1994, *Vasco et al.*, 2000]. One could also argue for a solution of the form (8) on physical grounds, based upon dimensional or similarity analysis of the equation for drawdown.

An asymptotic solution is obtained by substituting the series (8) into the governing equation (3). The resulting expression contains an infinite number of terms of increasing order in $1/\sqrt{i\omega}$. I shall be interested in the rapidly varying component of transient head , as is associated with the early increase in head due to the initiation of pumping. For ω large only the first few terms of the series (8) will be significant [*Kline and Kay*, 1965; *Kravtsov and Orlov*, 1990]. In particular, terms of order zero and one are typically considered in the expansion [*Virieux et al.*, 1994; *Vasco et al.*, 2000]. I should note that the term 'high-frequency' is relative to the length scale-of the heterogeneity. That is, I am assuming that the heterogeneity is smoothly varying when compared to the spatial scale over which the head increases from its background value to a significantly different value.

2.4. Computing Arrival Time Sensitivities

For terms of highest order in $\sqrt{i\omega}$, those of order $(\sqrt{i\omega})^2$, provide an equation for σ [*Virieux et al.*, 1994; *Vasco et al.*, 2000],

$$\nabla\sigma(\mathbf{x}) \cdot \nabla\sigma(\mathbf{x}) = \kappa(\mathbf{x}). \tag{10}$$

Equation (10), known as the eikonal equation, governs many types of propagation processes [*Kline and Kay*, 1965; *Kravtsov and Orlov*, 1990] and there are efficient direct numerical methods for its solutions [*Sethian*, 1996]. However, the method of characteristics may be used to convert the non-linear partial differential equation (10) into a system of linear, ordinary differential equations [*Courant and Hilbert*, 1962], the ray equations,

$$\frac{d\mathbf{X}}{ds} = \mathbf{p} \tag{11}$$

$$\frac{d\mathbf{p}}{ds} = \nabla\kappa \tag{12}$$

where $\mathbf{p} = \nabla\sigma$ and $\mathbf{X}(s)$ is a curve or trajectory through the model along which the solution is defined. The system of ordinary differential equations, along with a set of boundary conditions, can be solved using numerical techniques for two-point boundary-value problems [*Keller*, 1968]. Alternatively, as noted in *Vasco and Finsterle* [2004] one can use a numerical simulator to calculate σ and hence $\mathbf{p}$ and then solve (11) using a variation of a Runge-Kutta method [*Press et al.*, 1992] known as Heun's method [*Sethian*, 1996; *Vasco and Finsterle*, 2004]. In essence, one used a numerical simulator to calculate the arrive time of the head pulse peak at each point in the model, obtaining $\sigma(\mathbf{x})^2/6$. One computes $\mathbf{p}$ from the gradient of $\sigma(\mathbf{x})$ and formulates the differential equation (11). Numerically integrating (11) produces the trajectory $\mathbf{X}(s)$ along which the solution is defined.

The eikonal equation (10), written in ray coordinates, can be used to relate the pseudo-phase $\sigma(\mathbf{x})$ to the flow properties, as contained in $\kappa(\mathbf{x})$

$$\sigma(\mathbf{x}) = \int_{\Sigma(\mathbf{x})} \sqrt{\kappa(s)} ds \tag{13}$$

where the integral is along the path $\Sigma(\mathbf{x})$ from the source to the observation point. This integral relates $\sigma(\mathbf{x})$ directly to flow properties, $\kappa(s)$, integrated along the trajectory Σ. From equations (5) and (13) I may compute the sensitivity associated with the square root of the arrival time to changes in specific storage

$$\frac{\partial \sigma}{\partial S(\mathbf{x})} = \frac{\sqrt{\kappa(\mathbf{x})}}{S(\mathbf{x})} \tag{14}$$

and hydraulic conductivity

$$\frac{\partial \sigma}{\partial K(\mathbf{x})} = -\frac{\sqrt{\kappa(\mathbf{x})}}{K(\mathbf{x})} \tag{15}$$

[*Vasco et al.*, 2000]. Hence, a perturbation in arrival time is related to perturbations in $S(\mathbf{x})$ and $K(\mathbf{x})$ by

$$\delta\sigma(\mathbf{x}) = \int_{\Sigma(\mathbf{x})} \left[\frac{\sqrt{\kappa(s)}}{S(s)} \delta S(s) - \frac{\sqrt{\kappa(s)}}{K(s)} \delta K(s) \right] ds \tag{16}$$

where $\Sigma(\mathbf{x})$ is the trajectory between the pumping and observing boreholes. Note, the sensitivity in a homogeneous medium is uniform between the pumping and observing well. Unlike head amplitudes [*Oliver*, 1993], the arrival time sensitivities are not dominated by structure in the vicinity of the boreholes. As in medical and geophysical imaging, one may adopt a tomographic approach in order to invert the arrival times. Some initial reservoir model is assumed and the trajectories are traced through the model. By back-projecting the arrival time anomalies along the trajectories, I may estimate variations in storage and conductivity between the boreholes. A more detailed account of this approach will be given in the numerical illustration below.

2.5. Computing Amplitude Sensitivities

I begin the discussion of amplitude matching with a slight generalization of the lowest-order representation of the head variation, the zeroth-order term of equation (8),

$$H(\mathbf{x},\omega) = S(\omega) e^{-\sqrt{i\omega}\sigma(\mathbf{x})} A_0(\mathbf{x}) \tag{17}$$

where I have included a frequency-dependent quantity $S(\omega)$ which accounts for a time-varying source. This function is necessary in treating actual field data because the pumping rate will vary due to experimental conditions. While it is perfectly feasible to use the relationship between the quantities $\sigma(\mathbf{x})$ and $A_0(\mathbf{x})$ and the flow properties [*Vasco et al.*, 2000] to compute sensitivities for inverting amplitude data, I follow a different route. I use a high-frequency approximation, which involves much less computation and gives the lowest-order sensitivities [*Vasco et al.*, 2003]. Such an approach is appropriate for an initial matching of the amplitude data, following an arrival time inversion.

To invert transient head variations I require the sensitivities, relating perturbations in properties of the medium to perturbations in the observations. In what follows a quantity in the unperturbed medium is denoted by a circumflex. Thus, $\hat{\sigma}(\mathbf{x})$ and $\hat{A}_0(\mathbf{x})$ signify the phase and amplitude in the background medium. Given a perturbation of flow properties from their value in the background medium, I wish to compute the associated changes in the head variations.

In the perturbed medium the hydraulic conductivity is given by

$$K(\mathbf{x}) = \hat{K}(\mathbf{x}) + \delta K(\mathbf{x}) \tag{18}$$

where $\delta K(\mathbf{x})$ is the perturbation. Our transient head observations will likewise change as a result of the perturbation in hydraulic conductivity. I represent this change as a

perturbation δH to the head variation corresponding to the background medium $\hat{H}$:

$$H(\mathbf{x},\omega) = \hat{H}(\mathbf{x},\omega) + \delta H(\mathbf{x},\omega). \tag{19}$$

Given the particular form of the zeroth-order asymptotic solution, equation (17) , I consider perturbations in both phase

$$\sigma(\mathbf{x}) = \hat{\sigma}(\mathbf{x}) + \delta\sigma(\mathbf{x}) \tag{20}$$

and amplitude

$$A(\mathbf{x}) = \hat{A}_0(\mathbf{x}) + \delta A_0(\mathbf{x}) \tag{21}$$

resulting from a small change in the background hydraulic conductivity model. I may write the perturbed transient head variation $H(\mathbf{x},\omega)$ in terms of the expressions (20) and (21)

$$H(\mathbf{x},\omega) = e^{-\sqrt{i\omega}\hat{\sigma}} e^{-\sqrt{i\omega}\delta\sigma} S(\omega)(\hat{A}_0 + \delta A_0) \tag{22}$$

where I suppress the explicit $\mathbf{x}$ dependence until the final result. Expanding the exponential term in $\delta\sigma$ in a Taylor series, retaining only terms of first order in the perturbations, I find that

$$H(\mathbf{x},\omega) = e^{-\sqrt{i\omega}\hat{\sigma}} S(\omega)\hat{A}_0 - \sqrt{i\omega} e^{-\sqrt{i\omega}\hat{\sigma}} S(\omega)\hat{A}_0\delta\sigma$$

$$+ e^{-\sqrt{i\omega}\hat{\sigma}} S(\omega)\delta A_0. \tag{23}$$

Hence, making use of the fact that the head in the background medium is given by

$$\hat{H}(\mathbf{x},\omega) = S(\omega) e^{-\sqrt{i\omega}\hat{\sigma}(\mathbf{x})} \hat{A}_0(\mathbf{x}) \tag{24}$$

the perturbation $\delta H(\mathbf{x},\omega) = H(\mathbf{x},\omega) - \hat{H}(\mathbf{x},\omega)$, is given by

$$\delta H(\mathbf{x},\omega) = -\sqrt{i\omega} e^{-\sqrt{i\omega}\hat{\sigma}} S(\omega)\hat{A}_0\delta\sigma + e^{-\sqrt{i\omega}\hat{\sigma}} S(\omega)\delta A_0. \tag{25}$$

Note that the ω dependence is contained in the source-time function $S(\omega)$ and in the exponential phase term. The second term on the right of (25) contains the quantity δA_0 which relates a perturbation in flow properties to changes in the amplitude, as calculated from the transport equation [*Vasco et al.*, 2000]. Computing this quantity requires fairly involved ray-perturbation [*Keller*, 1962; *Moore*, 1991; *Norton and Linzer*, 1982; *Farra and Madariaga*, 1987 ; *Neele et al.*, 1993] or Born [*Vasco et al.*, 2000] approaches. However, for high-frequency (large ω) head variations, the first term on the right-hand-side of (25) will dominate. Thus, at high frequencies, I obtain a linearized relationship between the waveform perturbation in the frequency domain and the phase perturbation

$$\delta H(\mathbf{x},\omega) = -\sqrt{i\omega} e^{-\sqrt{i\omega}\hat{\sigma}(\mathbf{x})} S(\omega) \hat{A}_0(\mathbf{x}) \delta\sigma. \tag{26}$$

Note that, by discarding the second term on the right-hand-side of equation (25) I am neglecting amplitude perturbations due to scattering. This is a reasonable approximation when the scale-length of the heterogeneity is much larger than the wavelength of propagating wave. From equation (26) I may deduce the high-frequency sensitivity coefficients needed for inverting transient head amplitudes. Using equation (24), I may write equation (26) as

$$\delta H(\mathbf{x},\omega) = -\sqrt{i\omega} \hat{H}(\mathbf{x},\omega) \delta\sigma. \tag{27}$$

By inverse Fourier transforming the expression (27) I can derive a time-domain expression for the sensitivities. First I write $\sqrt{i\omega}$ as

$$\sqrt{i\omega} = (i\omega) \frac{1}{\sqrt{\pi}} \sqrt{\frac{\pi}{|\omega|}} \mathrm{e}^{-i \mathrm{sgn}(\omega) \frac{\pi}{4}} \tag{28}$$

and I note that [*Chapman*, 1985]

$$\mathcal{F}^{-1} \left\{ \frac{1}{\sqrt{\pi}} \frac{\pi}{|\omega|} \right\} = \frac{J(t)}{\sqrt{t\pi}} \tag{29}$$

where $J(t)$ is the Heaviside or step function which signifies a jump from zero to one at $t = 0$, [*Bracewell*, 1978]. And hence, taking into account the properties of the Fourier transform, mainly that multiplication by $i\omega$ in the frequency domain is equivalent to taking the time derivative, I arrive at the time-domain expression

$$\delta h(\mathbf{x},t) = -\frac{d}{dt}\left[\frac{J(t)}{\sqrt{\pi t}} * \hat{h}(\mathbf{x},t)\right]\delta\sigma. \tag{30}$$

where $*$ denotes a temporal convolution. If I define the function

$$F(\mathbf{x},t) = -\frac{d}{dt}\left[\frac{J(t)}{\sqrt{\pi t}} * \hat{h}(\mathbf{x},t)\right] \tag{31}$$

and make use of the expression for the phase perturbation $\delta\sigma(\mathbf{x})$, equation (16), I can write the amplitude sensitivity as

$$\delta h(\mathbf{x},t) = F(\mathbf{x},t)\int_{\Sigma(\mathbf{x})}\left[\frac{\sqrt{\kappa(s)}}{S(s)}\delta S(s) - \frac{\sqrt{\kappa(s)}}{K(s)}\delta K(s)\right]ds. \tag{32}$$

Summarizing the steps for computing the amplitude sensitivity based upon equations (32) and (31): First, compute the head variation in the background medium, perhaps with a numerical simulator. Then compute the phase function for the background medium, $\hat{\sigma}(\mathbf{x})$ and the trajectories $\Sigma(\mathbf{x})$, either by ray tracing or from the arrival time peak of the slope of the head curve. Convolve the head variation with the function in equation (29) and differentiate the result. The total sensitivity is then given by equation (32).

2.6. Use of the Logarithm to Ensure Positivity

In an iterative updating scheme the specific storage and/or hydraulic conductivity can take on negative values if the perturbations are large and negative. This violates the constraint that the flow properties are always positive, resulting in a non-physical solution. In this paper I ensure that the flow properties are always positive by formulating the iterative algorithm in terms of perturbations of the logarithm of specific storage and

hydraulic conductivity. Using the relationships

$$\delta \log S = \frac{1}{S}\delta S \tag{33}$$

$$\delta \log K = \frac{1}{K}\delta K \tag{34}$$

I can write equation (32) as

$$\delta h(\mathbf{x},t) = F(\mathbf{x},t)\int_{\Sigma(\mathbf{x})} \sqrt{\kappa(s)}\,[\delta \log S(s) - \delta \log K(s)]\,ds \tag{35}$$

where $\kappa(s)$ is the value in the background medium.

3. Applications

In this section I apply the iterative inversion technique to both synthetic and experimental head values. One aim of the numerical illustration is to determine how well one can match the transient head waveforms using the zeroth-order approach.

3.1. Numerical Illustration

A synthetic set of transient head values was generated using the numerical simulator TOUGH2 [*Pruess et al*, 1999]. The simulated transient test involves injection of water into a borehole intersecting a fracture zone. The properties of the test are intended to coincide with the general features of the Migration experiment, described below. The spatial distribution of hydraulic conductivity within the fracture zone is shown in Figure 1. Only hydraulic conductivity is allowed to varying in this test problem. Fluid is injected into well 9 in the figure and the head response is observed in the seven adjacent wells. The flow rate is constant after pumping is initiated, modeled by a step function in time. As noted in the Methodology section, I can calculate an arrival time from the output of a numerical simulator. Specifically, using the transient head variation from the simulation,

I can compute the time at which the head is changing most rapidly, the time at which the slope of the curve is greatest. In Figure 2 I plot the square root of this arrival time on the simulation grid. In addition, the trajectories, obtained by solving equation (11) using a Runge-Kutta technique, are shown as curved extending from the injection well to the observation wells.

An iterative updating scheme is used to invert the transient head values and to estimate the hydraulic conductivity within the fracture zone model. I start with a uniform conductivity distribution of 2.0×10^{-13} m^2 which is successively updated in order to better match the head arrival times. The head variation corresponding to the reference model (Figure 1) is indicated by the solid line (Obs) and unfilled squares in Figure 3. The head variation calculated using the initial uniform conductivity model is denoted by the dashed line in Figure 3. Initially, the amplitudes of the time-derivative of the transient head are under-predicted by several orders of magnitude. The sensitivities for the arrival time inversion are given in equation (15).

For a given step, the equation for the update is formulated as a least squares problem. That is, for a set of N phase residuals, $\delta\sigma_i, i = 1, 2, ..., N$, where the phase is computed from the arrival time of the peak slope via equation (9), I minimize the sum of the squares of the residuals [*Parker*, 1994]. An explicit expression may be obtained by combining equation (16) and equation (34) and discretizing the integral as a sum over the trajectory segments (Δs_{il}) in each grid block of the model

$$\delta\sigma_i = -\sum_{l=1}^{M} \sqrt{\kappa_{il}} \Delta s_{il} \delta \log K_l. \tag{36}$$

If I denote the coefficients of equation (36) by

$$G_{il} = -\sqrt{\kappa_{il}} \Delta s_{il} \tag{37}$$

then I can write equation (36) as

$$\delta\sigma_i = \sum_{l=1}^{M} G_{il}\delta \log K_l. \tag{38}$$

In this numerical illustration I discretized the two-dimensional fracture zone model into a 40 by 40 grid of cells, for a total of 1600 grid blocks. In the least-squares approach one finds the values of $\delta \log K_l$ that minimize the sum of the squares of the residuals [*Press et al*, 1992]

$$R^2 = \sum_{i=1}^{N} \left[\delta\sigma_i - \sum_{l=1}^{M} G_{il}\delta \log K_l \right]^2. \tag{39}$$

In this case, as in many inverse problems there are more unknown parameters ($M = 1600$) then there are data ($N = 7$). Thus, the inverse problem is under-determined and the solution is non-unique. That is, many solutions will re-produce the set of transient head residuals. One approach to treating the non-uniqueness introduces penalty terms which quantify some aspect of the model which one seeks to minimize [*Parker*, 1994]. For example, I can require that the model not deviate from a favored prior model, unless it is necessary to fit the transient head values. Thus, I can also minimize the sum of the squared deviations from a prior model ${K_i}^0, i = 1, 2, ..., M$, as measured by

$$B^2 = \sum_{i=1}^{M} \left[\log {K_i}^0 - (\log {K_i}^{current} + \delta \log K_i) \right]^2 \tag{40}$$

where ${K_i}^{current}$ is the current model of hydraulic conductivity. Another consideration is that the observational data cannot resolve small scale features of the model. Thus, one might only seek to determine the large scale variation in hydraulic conductivity. This suggests that one penalize solutions with rapid spatial variations in properties, e.g. rough models. A measure of model roughness is provided by the norm of the spatial gradient

vector of the model. I write it in the form

$$D^2 = \sum_{i=1}^{M} \left[\delta \log K_i \sum_{j=1}^{M} D_{ij} \delta \log K_j \right]^2 \tag{41}$$

where D_{ij} is a matrix which contains the product of a discrete matrix approximation of the spatial gradient operator. Note that the residual term R^2 and penalty terms B^2 and D^2 are quadratic forms in the model parameters. Hence, minimizing the quantity

$$T^2 = R^2 + W_b B^2 + W_d D^2, \tag{42}$$

will produce a linear system of equations for the perturbations $\delta \log K_i, i = 1, 2, ..., M$ which can be solved using any linear solver [*Press et al.*, 1992]. Here, W_b and W_d are coefficients controlling the relative importance of fitting the data and honoring the penalty terms. The coefficients W_b and W_d were estimated by trial and error, by running a number of test inversion and evaluating the fit to the data and the size and roughness of the resulting model perturbations. Because the system of equations is large and sparse I use the solver advocated by *Paige and Saunders* [1982].

Initially, an arrival time inversion is conducted, with 14 model updates to the homogeneous starting model. The reduction in the squared error is shown in Figure 4 as a function of the number of iterations in the updating scheme. The misfit is reduced by over an order of magnitude after 12 iterations and the misfit reduction seems to have leveled off. The resulting arrival time inversion result is shown in Figure 5, as multipliers to the logarithm of the hydraulic conductivity. The solution contains the high conductivity feature extending from the west of well 9 to the northwest, towards wells 5 and 10 (Figure 1). Overall, the arrival times are matched, as indicted in Figure 6, though the waveform amplitudes are still significantly under-predicted [Figure 7].

Using the arrival time inversion result as a starting model, I next match the transient head waveforms using

$$\delta h(\mathbf{x},t) = -F(\mathbf{x},t)\int_{\Sigma(\mathbf{x})}\sqrt{\kappa(s)}\delta \log K(s) ds, \tag{43}$$

a form of equation (35) appropriate for variations solely in hydraulic conductivity. As in the arrival time inversion, I include model norm and roughness penalty terms to mitigate the non-uniqueness. Equation (43) is written in discrete form and the inverse problem for $\delta \log K_j, j = 1, 2, ..., M$ is formulated as a penalized linear least squares problem. The non-linear problem is solved through iteration, building up a solution via a sequence of linearized inversions. The misfit reduction as a function of the number of iterations is shown in Figure 8. The squared error is reduced by approximately two orders of magnitude in a few iterations. The solution, plotted in Figure 9 as a gray scale plot, is similar in pattern to Figure 5, the arrival time inversion result. However, the magnitude of the heterogeneity is larger and there are differences in detail. For example, there is an extension of high conductivity to the northwest, extending from well 9 to well 11. The final waveform match is quite good, as shown in Figure 10. The poorest fit is in the slowly varying component, found after the peak, as might be expected for a high-frequency asymptotic solution.

3.2. The Migration Experiment at the Grimsel Rock Laboratory, Switzerland

The Migration experiment involved constant withdrawal of water from a fracture zone [*Solexperts*, 1989]. The test was conducted at the Swiss National Cooperative for the Storage of Radioactive Waste (NAGRA) Grimsel Rock Laboratory. The Grimsel facility is a collection of tunnels and boreholes situated in the interior of a mountain in the Bernese

Alps [*Mauldon et al.*, 1993]. The geometry of the test is identical to the well pattern of the synthetic illustration [Figure 1]. The eight wells intersected a zone of fractures, known as an S zone [*Vasco et al.*, 1997], which consists of a series of subparallel fractures striking northeast. The feature represents a shear zone that parallels the foliation of the host rock. Mylonite, cataclastite, and other gouge materials are found within the subfractures, which form a braided zone about 0.5 m in thickness [*Vasco et al.*, 1997].

Water was withdrawn from well 9 [Figure 1] at a rate of 340 mL/min for more than 35 days. The hydraulic head was observed in seven surrounding wells which intersected the fracture zone. Packers were used to isolate the response of the fracture zone and tests indicated that the fracture zone was not influenced by nearby fractures [*Mauldon et al.*, 1993]. The response of six wells containing useful data are shown in Figure 11, the numbering scheme corresponds to that in Figure 1. Because the data are several years old I did not have exact flow rates and therefore assumed that the injection rate behaved as a step function with a constant flow rate of 340 mL/min. Thus, there may be some error due to transient effects in the forward and inverse modeling.

Using the head data I conduct an iterative inversion in order to infer the hydraulic conductivity in the interwell region. The first step of the inversion procedure involves estimating and utilizing the arrival time of the head variation at each of the six surrounding boreholes. To do this I differenced the transient head variation in order to estimate its slope as a function of time. The estimated values, shown in Figure 12, are somewhat noisy, perhaps due to the fact that the sampling was not optimal for computing derivatives. However, the arrival time estimates are adequate for estimating the large scale variations

in hydraulic conductivity, given the significant variations in travel time to the various observation wells.

I conducted a penalized, iterative, least-squares inversion by minimizing the quantity (42), as described in the Numerical Illustration. The starting model consisted of uniform field of hydraulic conductivity values (2.0×10^{-13} m^2). The numerical simulator TOUGH2 [*Pruess et al.*, 1999] was used to compute the head variations and calculate the trajectories required for the sensitivity computations. The total squared arrival time misfit as a function of the number of iterative updates is shown in Figure 13. The squared error decreases by approximately an order of magnitude in twenty iterations. The pattern of hydraulic conductivity required to match the arrival times is shown in Figure 14. An elongated, high conductivity feature is found between wells 5 and 9 and low conductivity is placed between wells 7 and 11. Roughly five orders of magnitude of variation in hydraulic conductivity is necessary in order to fit the observations. The initial and final fits to the arrival time data is shown in Figure 15. Generally, the data are matched fairly well, though the large travel time associated with well 11 still deviates from the observed value.

The next step in the inversion procedure involves matching the transient head waveforms. For this task, I start with the hydraulic conductivity model derived from the arrival time inversion (Figure 14). A penalized, iterative, least squares updating algorithm is used to find perturbations $\delta \log K_j, j = 1, 2, ..., M$ which improve the fit to the transient head waveforms. The total squared error as a function of the number of updates is shown in Figure 16. The total squared error decreases from 3.38 to 2.08, roughly 38%, in ten iterations before leveling off. There is still significant waveform misfit at the conclusion of the updating, perhaps due to errors in specifying the flowrate time variation. The final

conductivity estimates, shown in Figure 17, are similar to the values found by inverting the arrival times (Figure 14). The waveforms change dramatically during the inversion, as shown in Figures 18 and 19. Initially, the head derivative pulses are fairly similar in form, as shown in Figure 18. After arrival time and waveform matching, the head derivatives are significantly different in shape (Figure 19) and better match the observed variations (Figure 12).

4. Conclusions

The asymptotic formulation presented in this paper provides an efficient approach to transient head inversion. The inverse problem partitions into an arrival time matching problem and an amplitude or waveform matching problem. The inversion of arrival times was discussed previously by *Vasco et al.* [2000] and *Vasco and Finsterle* [2004]. This work is an extension of the trajectory-based approach to the inversion of transient head waveforms. The technique, which is similar to one applied in seismic waveform inversion [*Vasco et al.*, 2003], is a high frequency approximation requiring little more computation than arrival time inversion. Thus, it is an alternative to the more accurate Born-based technique described in *Vasco et al.* [2000] and to ray-perturbation techniques used in geophysics [*Norton and Linzer*, 1982; *Farra et al.*, 1987; *Moore*, 1991, *Neele et al.*, 1993]. As shown above, the methodology can take advantage of an existing numerical simulator to compute the trajectories and, ultimately, the sensitivities necessary for inverting transient head data.

The high frequency, trajectory-based waveform sensitivities are essentially re-weighted arrival time sensitivities. As such, the information provided by waveform sensitivities overlaps with that provided by arrival time data. However, the sensitivities provide addi-

tional flexibility in interpreting transient head observations because they do not require the estimation of an arrival time. Thus, in situations in which it might be difficult to compute arrival times, it is possible to work directly with the transient head data. For example, when there is interference between two pumping wells, or possibly due to multiple propagation paths from a source well to an observation point, as noted by *Vasco et al.* [2003]. The high frequency method is useful in deriving an initial model which can serve as the starting point for a more accurate waveform inversion. As shown in *Cheng et al.* [2005], such an initial model can be important due to the increased non-linearity associated with waveform inversion. The method should prove useful in situations in which there are large amounts of data, such as multilevel samplers and pressure transducers [*Freyberg*, 1986; *Butler et al.*, 1999] and crosswell pressure testing [*Hsieh et al.*, 1985; *Paillet*, 1993; *Cook*, 1995; *Masumoto et al.*, 1995; *Karasaki et al.*, 2000; *Yeh and Liu*, 2000; *Vesselinov et al.*, 2001].

The technique is a high frequency method which is appropriate for the initial portion of the transient head curve. As such, the approach is complementary to techniques which utilize low frequency information, such as static head changes. By combining data from the low and high frequency regimes one can estimate both hydraulic conductivity and specific storage. Such joint inversions will be the subject of future work on the interpretation of transient head observations.

Acknowledgments. This work was supported by the Assistant Secretary, Office of Basic Energy Sciences of the U. S. Department of Energy under contract DE-AC03-

76SF00098. All computations were carried out at the Center for Computational Seismology, Berkeley Laboratory.

References

Bear, J., *Dynamics of Fluids in Porous Media*, Dover Publications, 1972.

Bohling, G. C., X. Zhan, J. J. Butler, and L. Zheng, Steady shape analysis of tomographic pumping tests for characterization of aquifer heterogeneities, *Water Resour. Res.*, **38**, 60-1-15, 2002.

Bracewell, R. N., *The Fourier Transform and Its Applications*, McGraw-Hill, New York, 1978.

Brauchler, R., R. Liedl, and P. Dietrich, A travel time based hydraulic tomographic approach, *Water Resour. Res.*, **39**, 20-1-12, 2003.

Butler, J. J., Pumping tests in nonuniform aquifers-The radially symmetric case, *J. of Hydrology*, **101**, 15-30, 1988.

Butler, J. J., C. D., McElwee, and G. C. Bohling, Pumping tests in networks of multilevel sampling wells: Motivation and methodology, *Water Resour. Res.*, **35**, 3553-3560, 1999.

Chapman, C. H., Ray theory and its extensions, *J. Geophys.*, **58** 27-43, 1985.

Cheng, H., Z., He, and A. Datta-Gupta, A comparison of travel-time and amplitude matching for field-scale production data integration: Sensitivity, non-linearity, and practical implications, *Soc. Petrol. Eng. Journal*, **10**, 75-90, 2005.

Cohen, J. K., and R. M. Lewis, A ray method for the asymptotic solution of the diffusion equation, *J. Inst. Maths. Applics.*, **3** 266-290, 1967.

Courant, R., and D. Hilbert, *Methods of Mathematical Physics*, Interscience, New York, 1962.

Cook, P. J., *Analysis of Interwell Hydraulic Connectivity in Fractured Granite*, M. S. thesis, University of California, Berkeley, 1995.

de Marsily, G., *Quantitative Hydrogeology*, Academic Press, San Diego, 1986.

Farra, V., and R. Madariaga. Seismic waveform modeling in heterogeneous media by ray perturbation theory, *J. Geophys. Res.*, **92**, 2697-2712, 1987.

Freyberg, D. L., A natural gradient experiment on solute transport in a sand aquifer, 2, Spatial moments and the advection and dispersion of nonreactive tracers, *Water Resour. Res.*, **22**, 2031-2046, 1986.

He, Z., A. Datta-Gupta, and D. W. Vasco, Rapid inverse modeling of pressure interference tests using trajectory-based traveltime and amplitude sensitivities, *Water Resour. Res.*, **42**, 1-15, 2006.

Hsieh, P. A., S. P. Neuman, G. K. Stiles, and E. S. Simpson, Field determination of the three-dimensional hydraulic conductivity tensor of anisotropic media, 2, Methodology and application to fractured rocks, *Water Resour. Res.*, **21**, 1667-1676, 1985.

Jacquard, P., and C. Jain, Permeability distribution from field pressure data, *Soc. Petrol. Eng.*, **5**, 281-294, 1965.

Keller, H. B., *Numerical Methods for Two-Point Boundary-Value Problems*, Blaisdell, Waltham, MA, 1968.

Karasaki, K., B. Freifeld, A. Cohen, K. Grossenbacher, P. Cook, and D. Vasco, A multi-disciplinary fractured rock characterization study at the Raymond field site, Raymond California, *J. hydro.*, **236**, 17-34, 2000.

Keller, J. B, Wave propagation in random media, *Proc. Symp. Appl. Math.*, **13**, 227-246, 1962.

Kline, M., and I. W. Kay, *Electromagnetic Theory and Geometrical Optics*, John Wiley and Sons, 1965.

Kravtsov, Y. A., and Y. I. Orlov, *Geometrical Optics of Inhomogeneous Media*, Springer-Verlag, Berlin, 1990.

Masumoto, K., H., Tosaka, K. Kojimi, K. Itoh, and Y. Otsuka, New measuring system and high speed three dimensional inversion method for hydropulse tomography, in *8th International Congress on Rock Mechanics*, edited by T. Fuji, 847-850, A. A. Balkema, Brookfield, Vt., 1995.

Mauldon, A. D., K. Karasaki, S. J. Martel, J. C. S. Long, M. Landsfeld, A. Mensch, and S. Vomvoris, An inversion technique for developing models for fluid flow in fracture systems using simulated annealing, *Water Resour. Res.*, **29**, 3775-3789, 1993.

Moore, B. J., Seismic rays in media with slight lateral variation in velocity, *Geophys. J. Int.*, **105**, 213-227, 1991.

Neele, F., J. C. VanDecar, and R. Snieder, A formalism for including amplitude data in tomographic inversions, *Geophys. J. Int.*, **115**, 482-496, 1993.

Norton, S. J., and M. Linzer, Correcting for ray refraction in velocity and attenuation tomography: A perturbation approach, *Ultrason. Imag.*, **4**, 201-233, 1982.

Oliver, D. S., The influence of nonuniform transmission and storativity on drawdown, *Water Resour. Res.*, **29**, 169-178, 1993.

Paige, C. C., and Saunders, M. A., LSQR: An algorithm for sparse linear equations and sparse linear systems, *ACM Trans. Math. Software*, **8**, 195-209, 1982.

Paillet, F. L., Using borehole geophysics and cross-borehole flow testing to define connections between fracture zones in bedrock aquifers, *J. Appl. Geophys.*, **30**, 261-279, 1993.

Parker, R. L., *Geophysical Inverse Theory*, Princeton University Press, 1994.

Press, W. H., S. A. Teukolsky, W. T. Vetterling, and B. P. Flannery, *Numerical Recipes*, Cambridge University Press, Cambridge, 1992.

Pruess, K., C. Oldenburg, and G. Moridis, *TOUGH2 User's Guide, Version 2.0*, LBNL Report, **43134**, Berkeley, 1999.

Sethian, J. A., *Level Set Methods*, Cambridge University Press, 1996.

Solexperts, Nagra Migration Long Term Constant Q Test in BOMI 87.009, Test Analysis and Description, *Solexperts Report*, **566**, Zurich, 1989.

Sun, N.-Z., *Inverse Problems in Groundwater Modeling*, Kluwer Acad., Norwell Mass, 1994.

Tarantola, A., *Inverse Problem Theory: Methods for Data Fitting and Model Parameter Estimation*, Elsevier Sci, 1992.

Tikhonov, A. N., Mathematical basis of the theory of electromagnetic soundings, *USSR Comput. Math. and Math. Phys.*, **5**, 207-211, 1965.

Vasco, D. W., and A. Datta-Gupta, Asymptotic solutions for solute transport: A formalism for tracer tomography, *Water Resour. Res.*, **35**, 1-16, 1999.

Vasco, D. W., and Finsterle, S., Numerical trajectory calculations for the efficient inversion of flow and tracer observations, *Water Resour. Res.*, **40**, W01507, 1-17, 2004.

Vasco, D. W., Datta-Gupta, A., and Long, J. C. S., Resolution and uncertainty in hydrologic characterization, *Water Resour. Res.*, **33**, 379-397, 1997.

Vasco, D. W., H. Keers, and K. Karasaki, Estimation of reservoir properties using transient pressure data: An asymptotic approach, *Water Resour. Res.*, **36**, 3447-3465, 2000.

Vasco, D. W., H. Keers, J. E. Peterson, and E. Majer, Zeroth-order asymptotics: Waveform inversion of the lowest degree, *Geophysics*, **68**, 614-628, 2003.

Vesselinov, V. V., S. P. Neuman, and W. A. Illman, Three-dimensional numerical inversion of pneumatic cross-hole tests in unsaturated fractured tuff 2. Equivalent parameters high-resolution stochastic imaging, and scale effects, *Water Resour. Res.*, **37**, 3001-3017, 2001.

Virieux, J., C. Flores-Luna, and D. Gibert, Asymptotic theory for diffusive electromagnetic imaging, *Geophys. J. Int.*, **119**, 857-868, 1994.

Yeh, T.-C. J. and S. Liu, Hydraulic tomography: Development of a new aquifer test method, *Water Resour. Res.*, **36**, 2095-2105, 2000.

Figure 1. Hydraulic conductivity variation used for numerical trajectory computations. The well locations are denoted by open circles and well numbers. Well 9 serves as the pumping well for the calculations.

Figure 2. Contour plot of the square root of the arrival time of the peak in the head derivative. The contour units are in 0.01 days. The computed trajectories, connecting each observation well to the pumping well (9) are shown as solid lines.

Figure 3. Observed (solid line) and calculated (dashed line) time derivatives of the transient head variation at each of the observation wells in Figure 1.

Figure 4. Squared misfit to the arrival times as a function of the number of updates in the iterative inversion algorithm.

Figure 5. Hydraulic conductivity logarithm multipliers resulting from an inversion of the arrival times. The multipliers are plotted as a gray-scale variation, the open circles denote the observation wells, the open star indicates the pumping well.

Figure 6. Observed square root of the arrival time (horizontal axis) plotted against the calculated square root of the arrival time (vertical axis). For a perfect match the points would like upon the 45^o line plotted in the figure.

Figure 7. Observed (solid line) and calculated (dashed line) time derivatives of the transient head variation at each of the observation wells in Figure 1. The calculated head values are computed using the result of the arrival time inversion.

Figure 8. Total squared waveform misfit as a function of the number of iterations of the waveform matching algorithm.

Figure 9. Hydraulic conductivity logarithm multipliers resulting from an inversion of the transient head waveforms. The multipliers are plotted as a gray-scale variation, the open circles denote the observation wells, the open star indicates the pumping well.

Figure 10. Observed (solid line) and calculated (dashed line) time derivatives of the transient head variation at each of the observation wells in Figure 1. The calculated head values are computed using the result of the transient head waveform inversion.

Figure 11. Pressure changes for the six observation wells as a function of the square root of the time. The well numbers correspond to the locations shown in Figure 1.

Figure 12. The time derivative of the transient pressure observations from the Migration (MI) experiment. The horizontal scale is the square root of time.

Figure 13. Total squared waveform misfit as a function of the number of iterations of the Migration experiment arrival time inversion algorithm.

Figure 14. Hydraulic conductivity logarithm multipliers resulting from an inversion of the migration experiment arrival times. The multipliers are plotted as a gray-scale variation, the open circles denote the observation wells, the open star indicates the pumping well.

Figure 15. Observed square root of the arrival time (horizontal axis) plotted against the calculated square root of the arrival time (vertical axis) for the Migration experiment. For a perfect match the points would like upon the 45^o line plotted in the figure.

Figure 16. Total squared waveform misfit as a function of the number of iterations of the Migration experiment waveform inversion algorithm.

Figure 17. Hydraulic conductivity logarithm multipliers resulting from an inversion of the migration experiment waveform data. The multipliers are plotted as a gray-scale variation, the open circles denote the observation wells, the open star indicates the pumping well.

Figure 18. Transient head derivatives, calculated using a homogeneous initial model with a constant hydraulic conductivity of $2\times\ 10^{-13}$ m/s.

Figure 19. Transient head derivatives, calculated using the final waveform inversion conductivity model (Figure 17). The horizontal axis represents the square root of time.

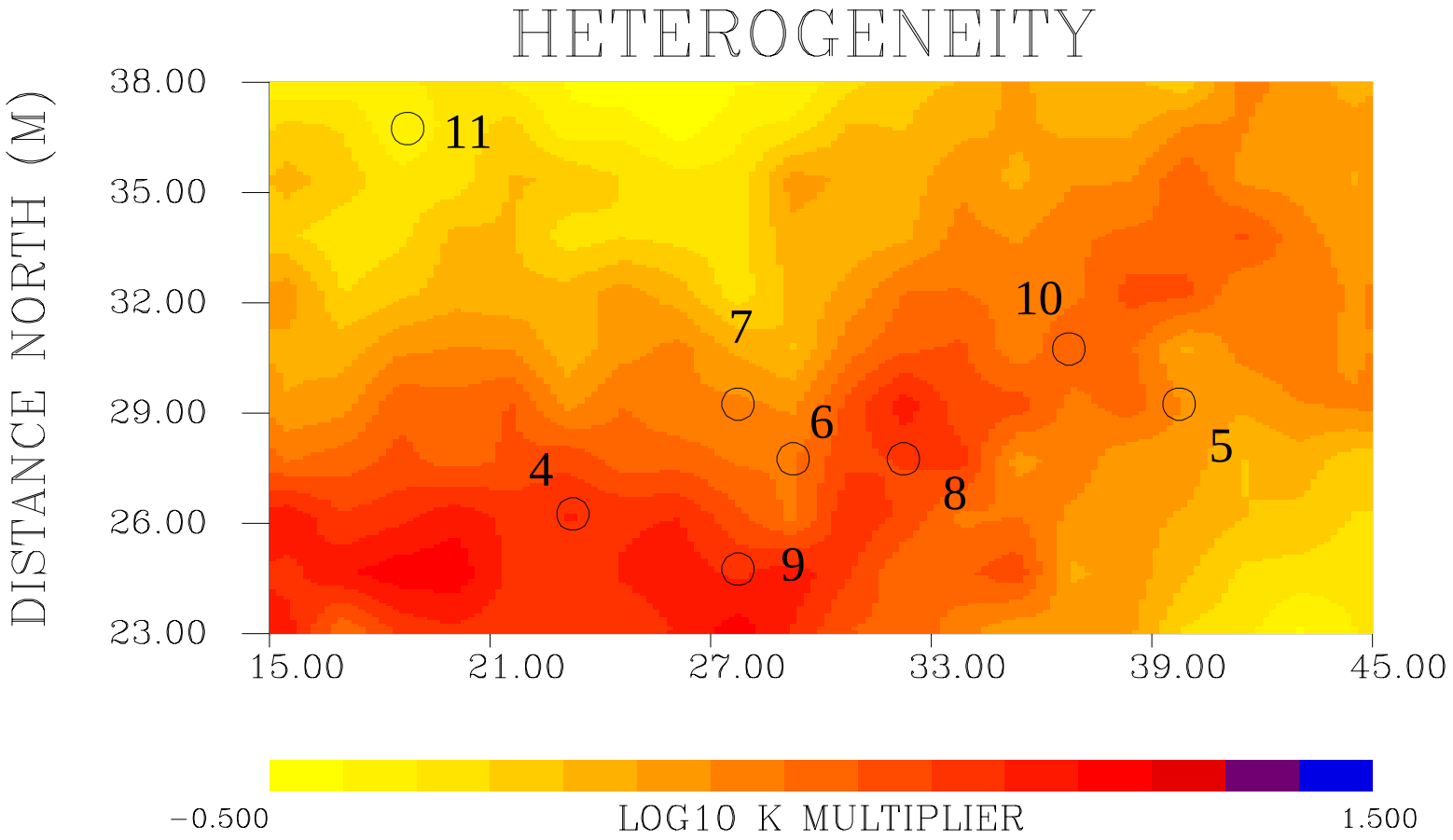
HETEROGENEITY
DISTANCE NORTH (M)
38.00
35.00
32.00
29.00
26.00
23.00
15.00
21.00
27.00
33.00
39.00
45.00
11
7
10
6
5
4
8
9
−0.500
LOG10 K MULTIPLIER
1.500

Figure 1.

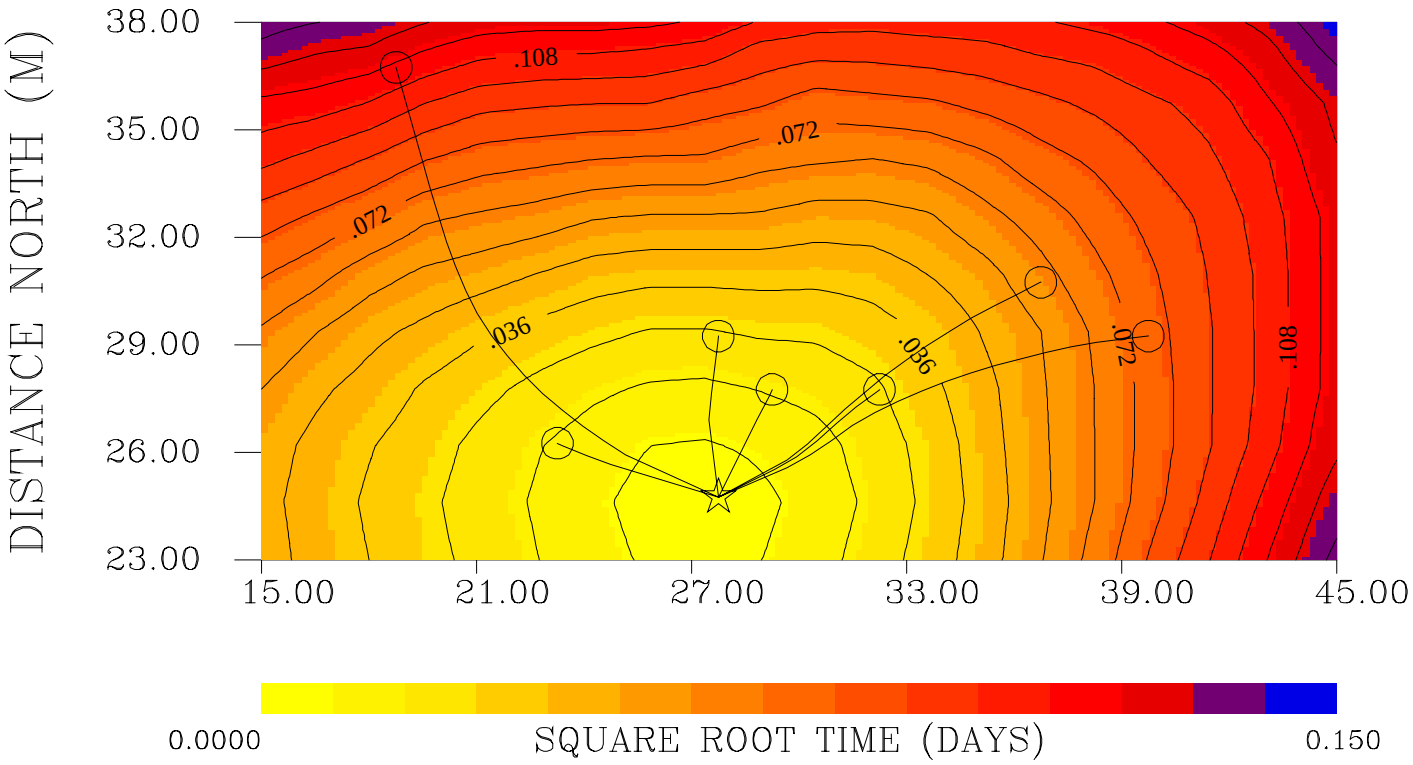
DISTANCE NORTH (M)
38.00
35.00
32.00
29.00
26.00
23.00
15.00
21.00
27.00
33.00
39.00
45.00
.108
.072
.072
.036
.036
.072
.108
0.0000
SQUARE ROOT TIME (DAYS)
0.150

Figure 2.

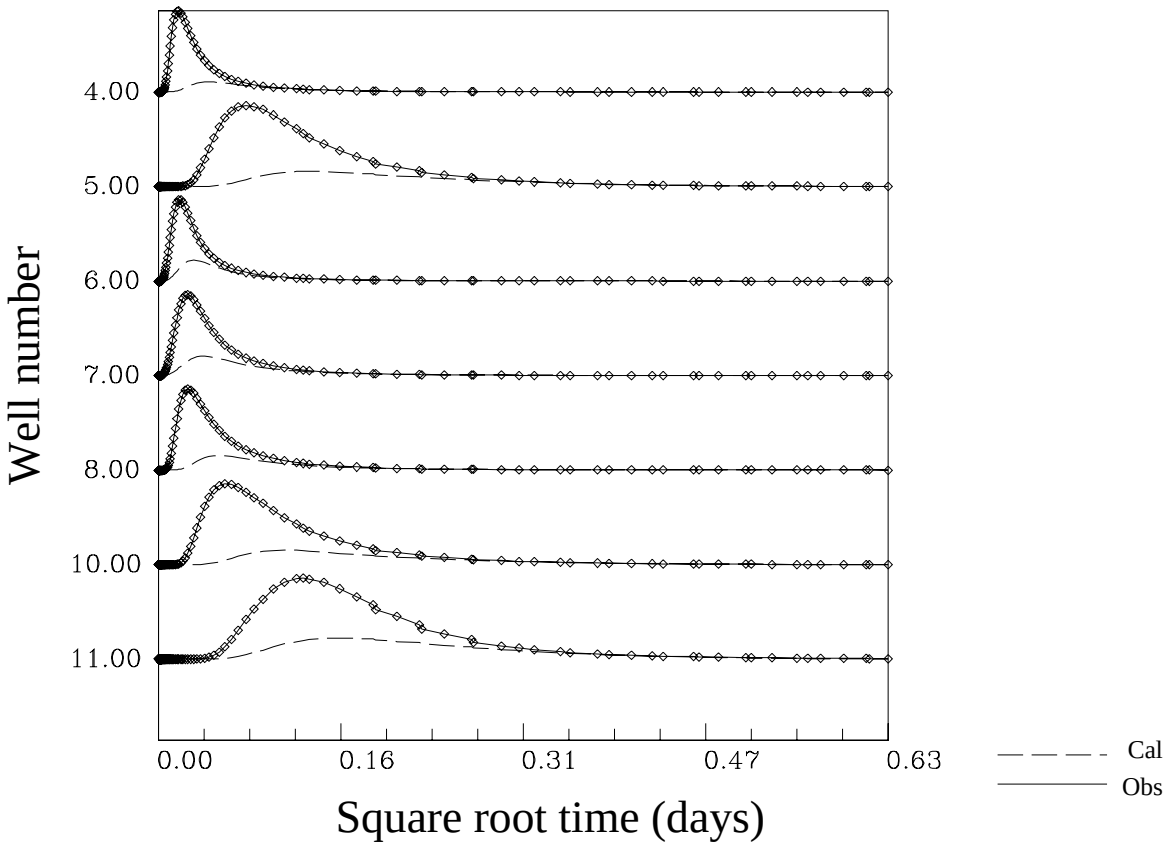
Well number
4.00
5.00
6.00
7.00
8.00
10.00
11.00
0.00
0.16
0.31
0.47
0.63
Square root time (days)
Cal
Obs

Figure 3.

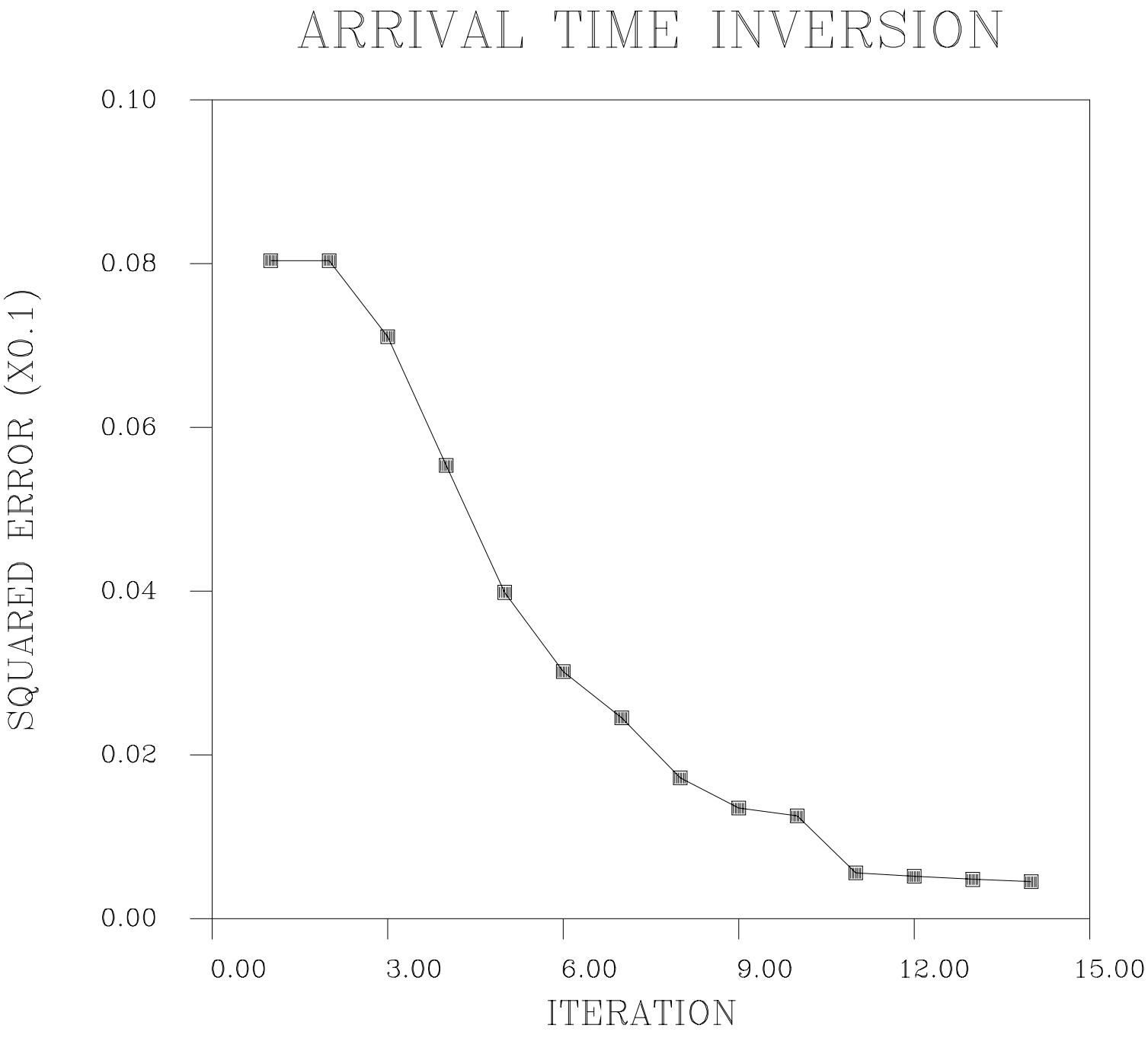
ARRIVAL TIME INVERSION
SQUARED ERROR (X0.1)
0.10
0.08
0.06
0.04
0.02
0.00
0.00
3.00
6.00
9.00
12.00
15.00
ITERATION

Figure 4.

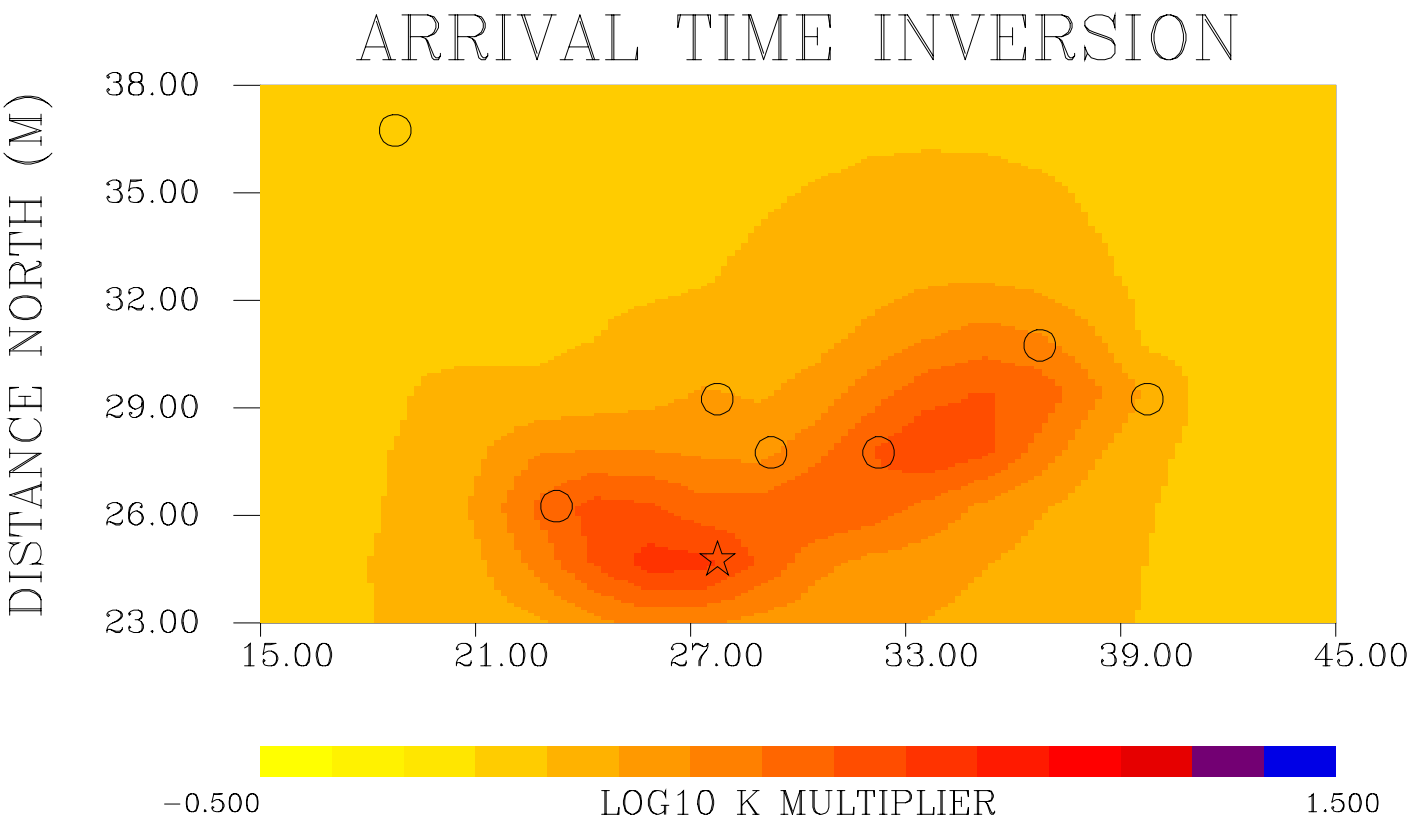
ARRIVAL TIME INVERSION
DISTANCE NORTH (M)
38.00
35.00
32.00
29.00
26.00
23.00
15.00
21.00
27.00
33.00
39.00
45.00
−0.500
LOG10 K MULTIPLIER
1.500

Figure 5.

Figure 6

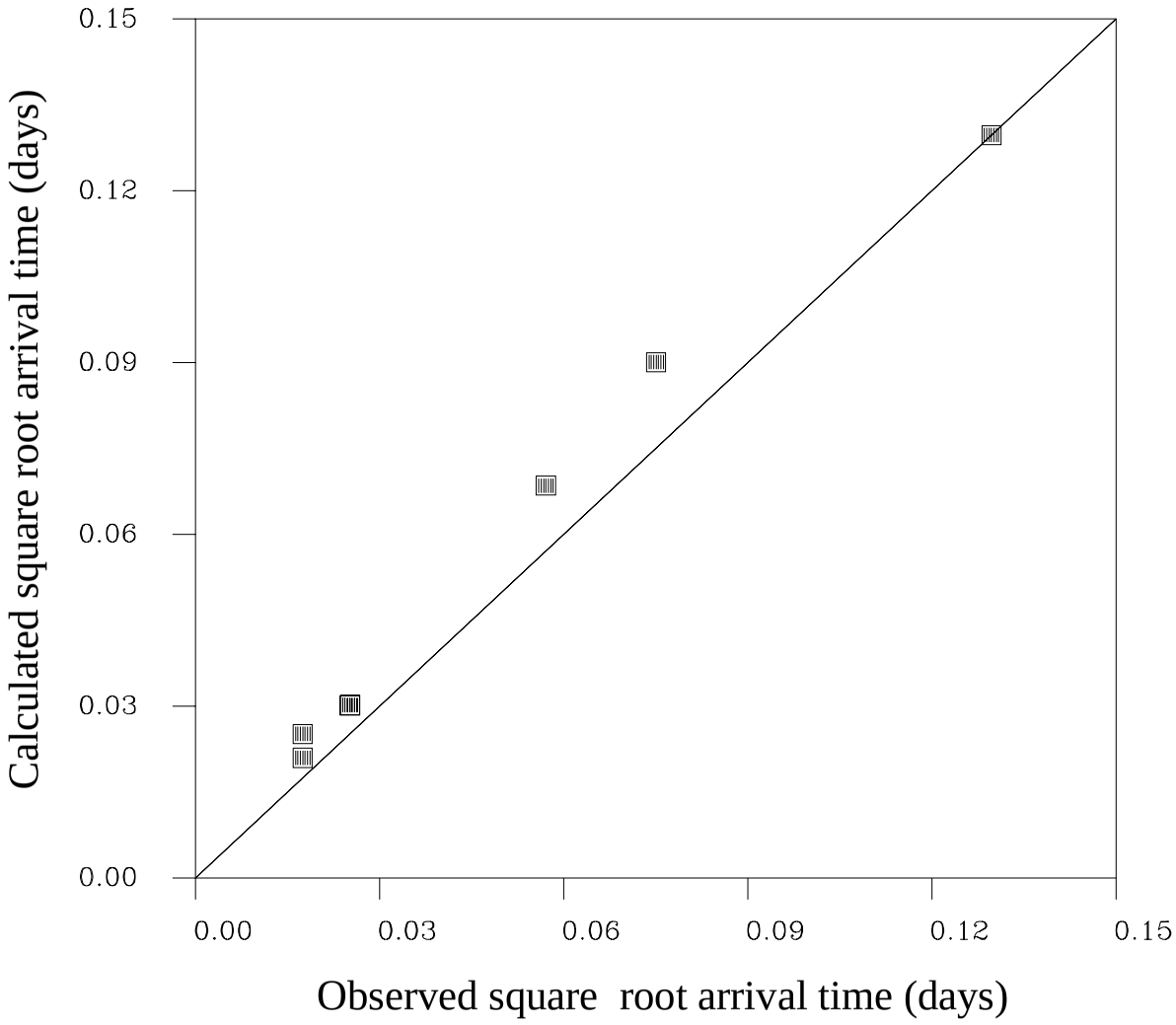
Calculated square root arrival time (days)
0.15
0.12
0.09
0.06
0.03
0.00
0.00
0.03
0.06
0.09
0.12
0.15
Observed square root arrival time (days)

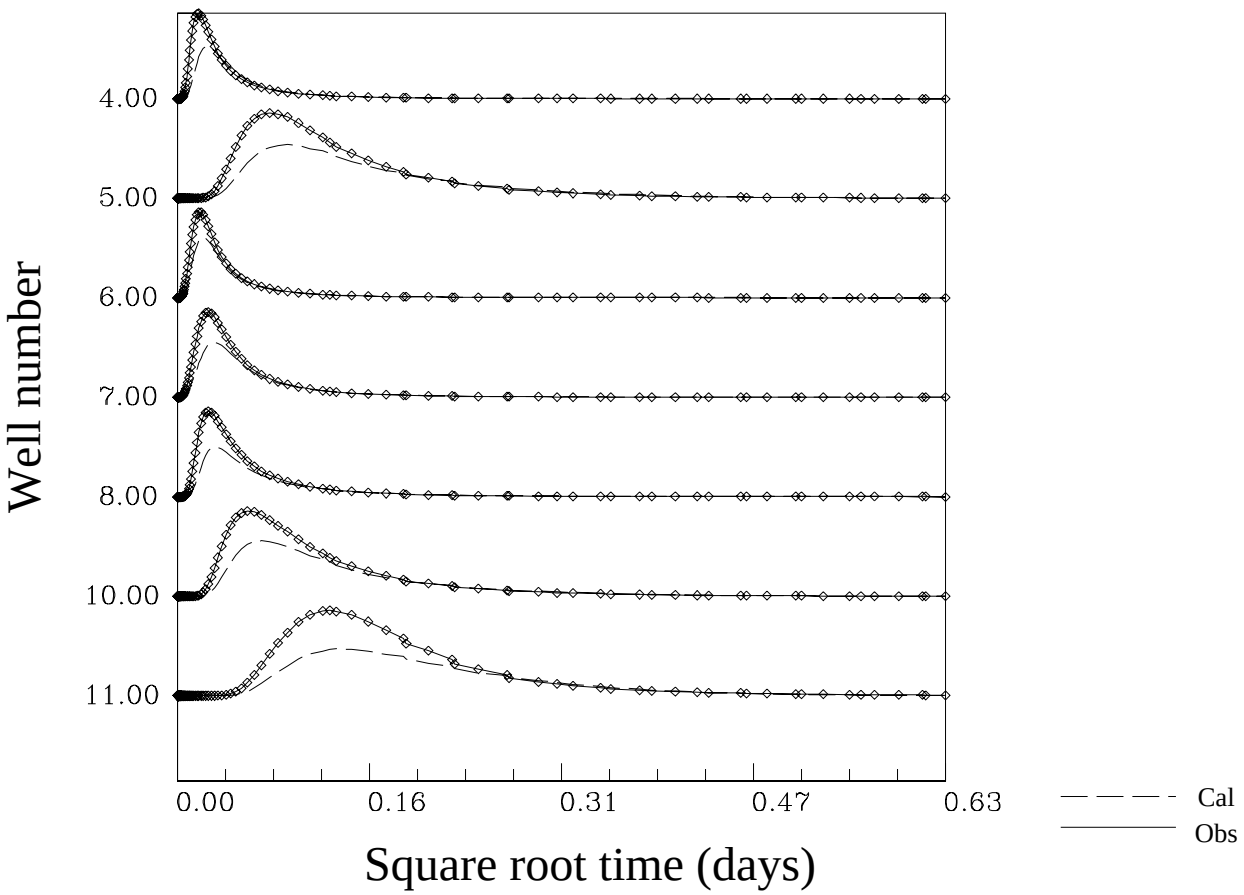
Well number
4.00
5.00
6.00
7.00
8.00
10.00
11.00
0.00
0.16
0.31
0.47
0.63
Square root time (days)
Cal
Obs

Figure 7.

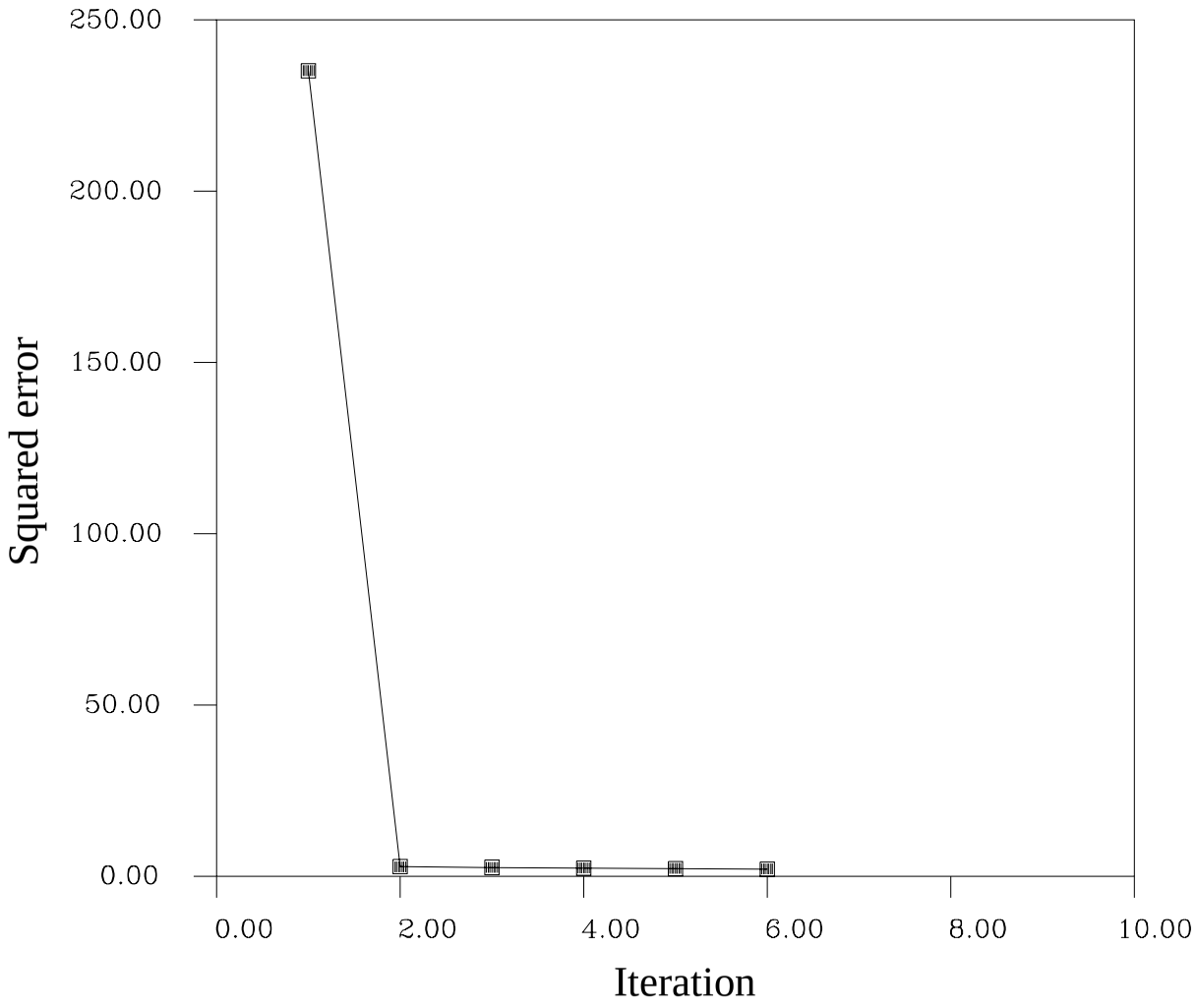
250.00
200.00
150.00
100.00
50.00
0.00
Squared error
0.00
2.00
4.00
6.00
8.00
10.00
Iteration

Figure 8.

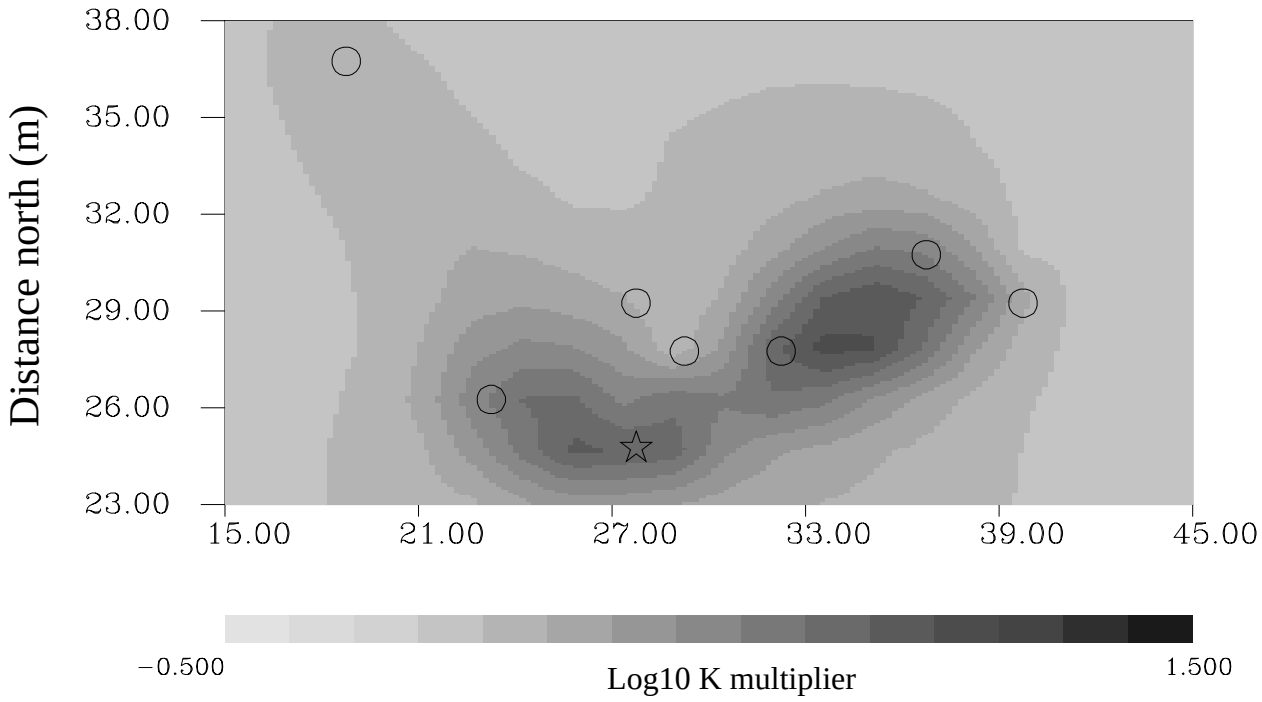
38.00
35.00
32.00
29.00
26.00
23.00
Distance north (m)
15.00
21.00
27.00
33.00
39.00
45.00
−0.500
1.500
Log10 K multiplier

Figure 9.

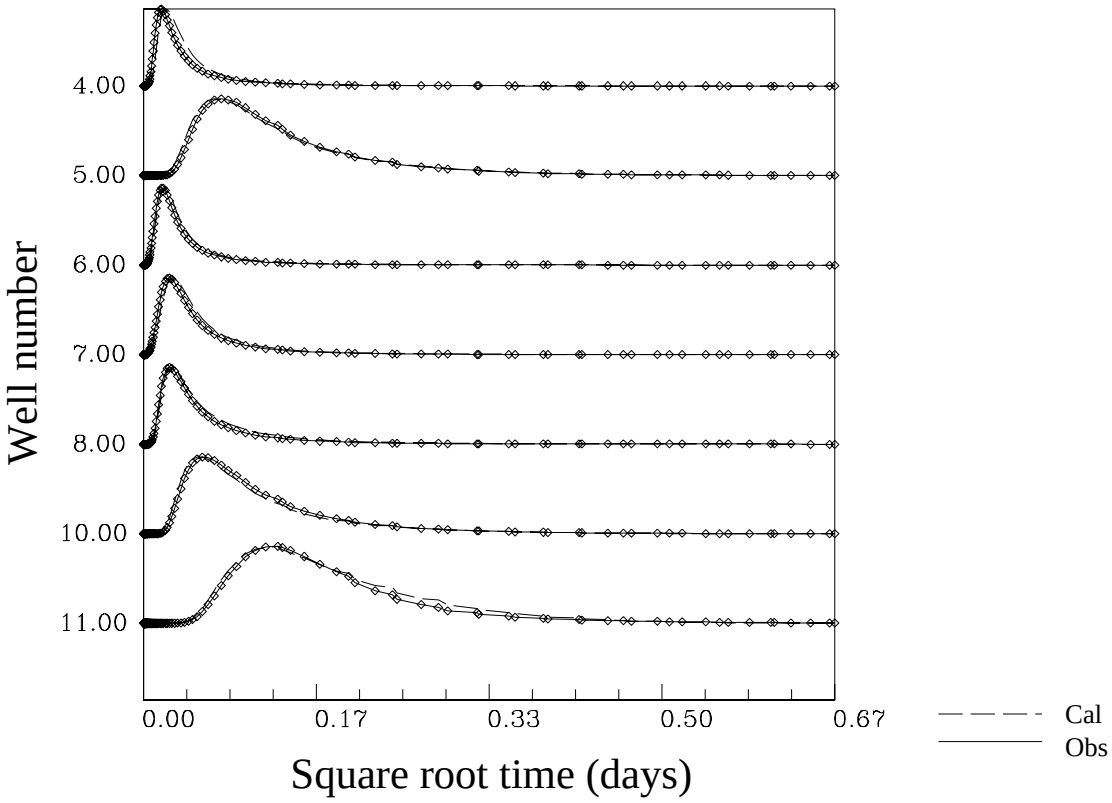
Well number
4.00
5.00
6.00
7.00
8.00
10.00
11.00
0.00
0.17
0.33
0.50
0.67
Square root time (days)
Cal
Obs

Figure 10.

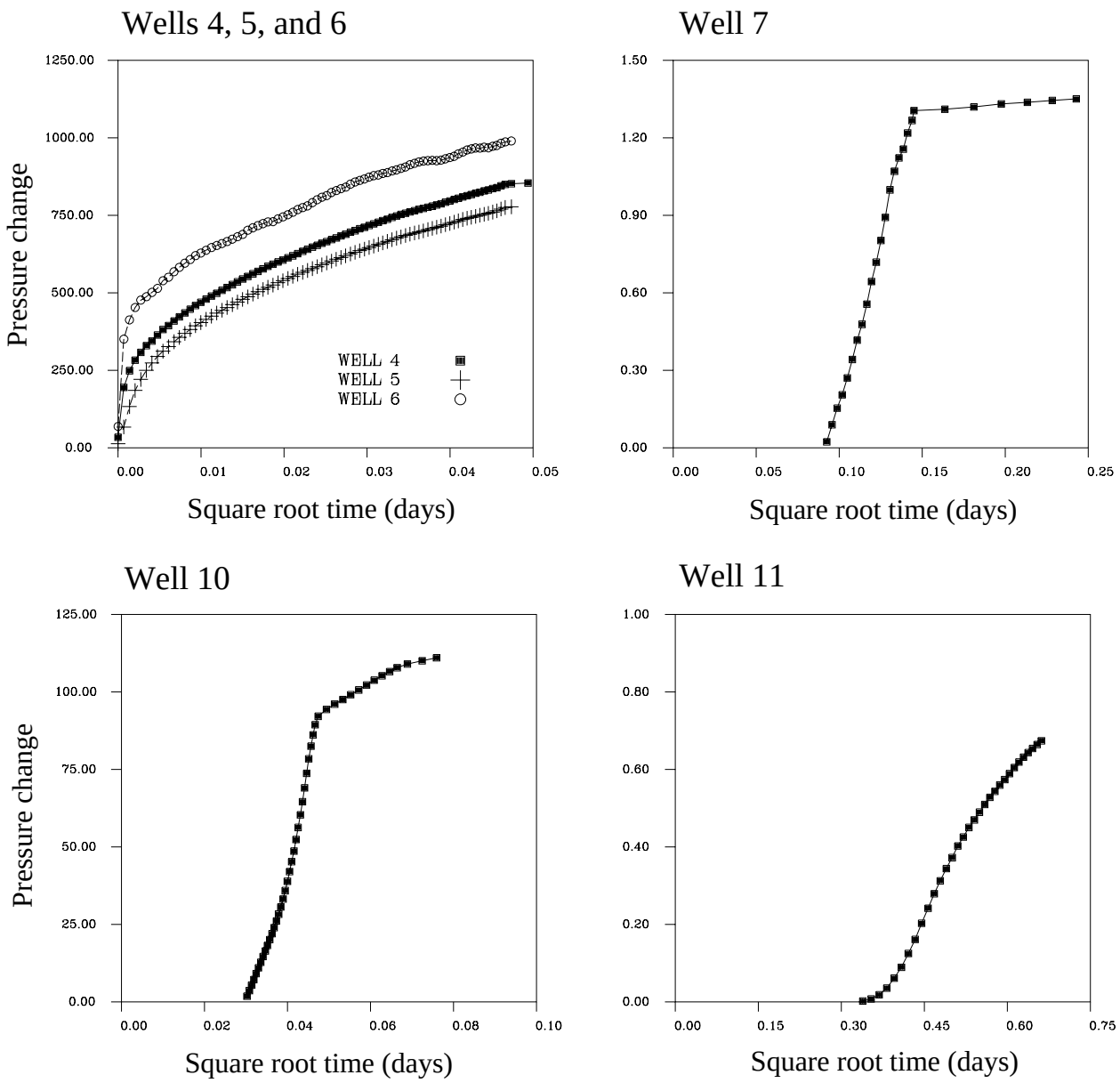
Wells 4, 5, and 6
Pressure change
1250.00
1000.00
750.00
500.00
250.00
0.00
0.00
0.01
0.02
0.03
0.04
0.05
WELL 4
WELL 5
WELL 6
Square root time (days)
Well 7
1.50
1.20
0.90
0.60
0.30
0.00
0.00
0.05
0.10
0.15
0.20
0.25
Square root time (days)
Well 10
Pressure change
125.00
100.00
75.00
50.00
25.00
0.00
0.00
0.02
0.04
0.06
0.08
0.10
Square root time (days)
Well 11
1.00
0.80
0.60
0.40
0.20
0.00
0.00
0.15
0.30
0.45
0.60
0.75
Square root time (days)

Figure 11.

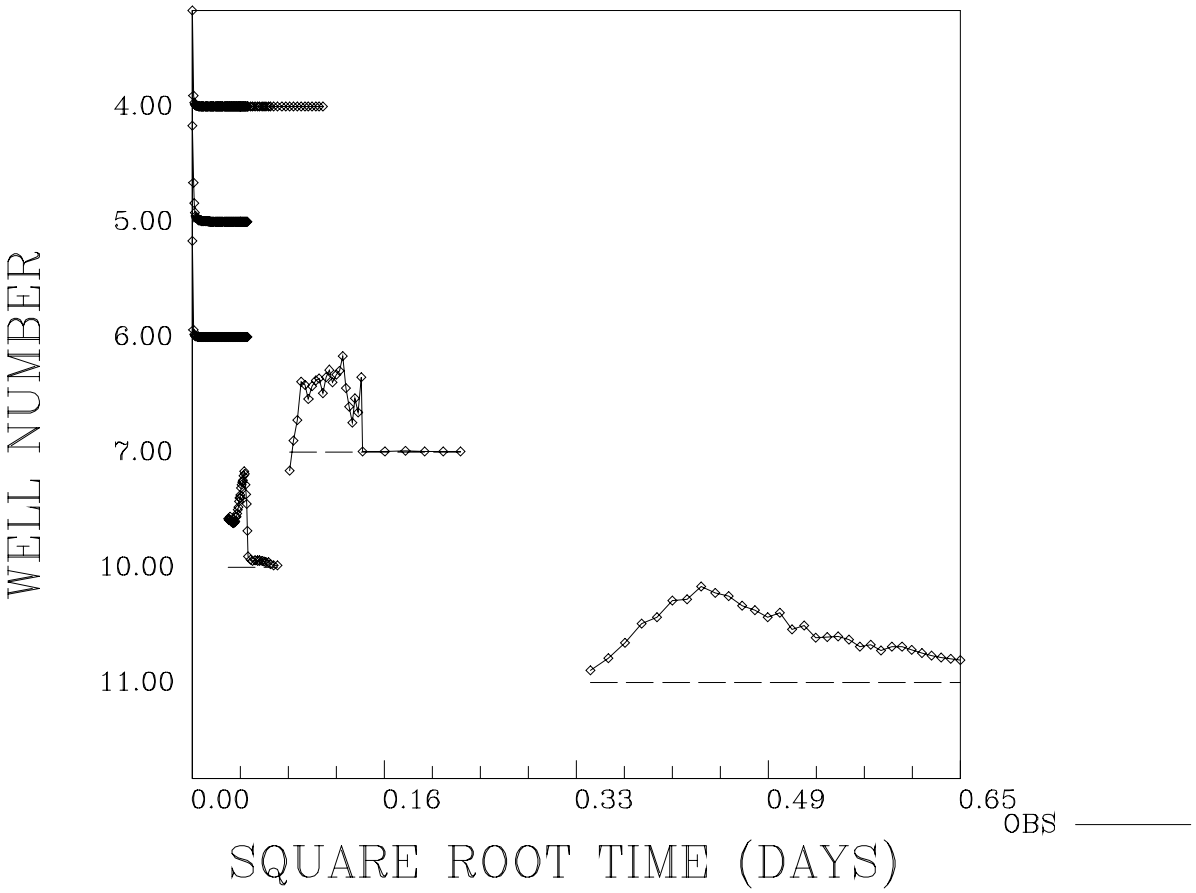
WELL NUMBER
4.00
5.00
6.00
7.00
10.00
11.00
0.00
0.16
0.33
0.49
0.65
OBS
SQUARE ROOT TIME (DAYS)

Figure 12.

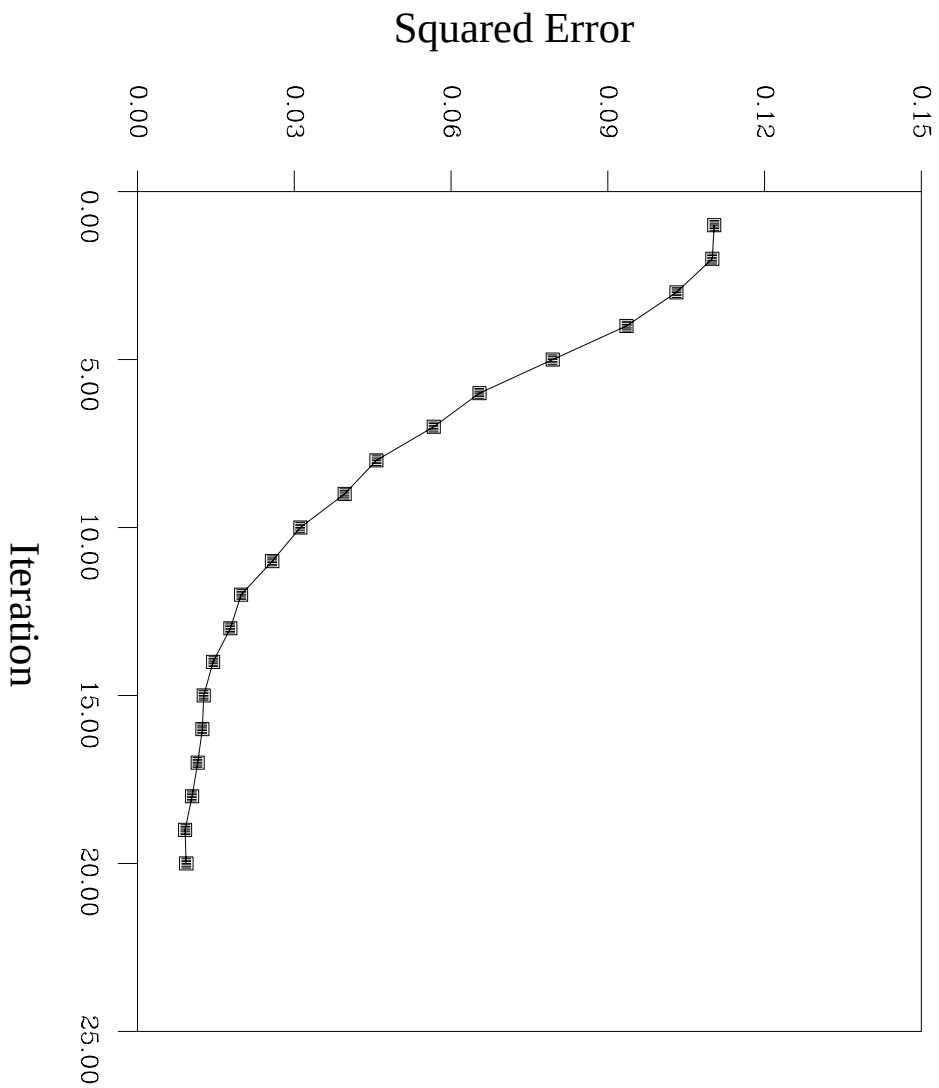
Squared Error
0.00
0.03
0.06
0.09
0.12
0.15
Iteration
0.00
5.00
10.00
15.00
20.00
25.00

Figure 13.

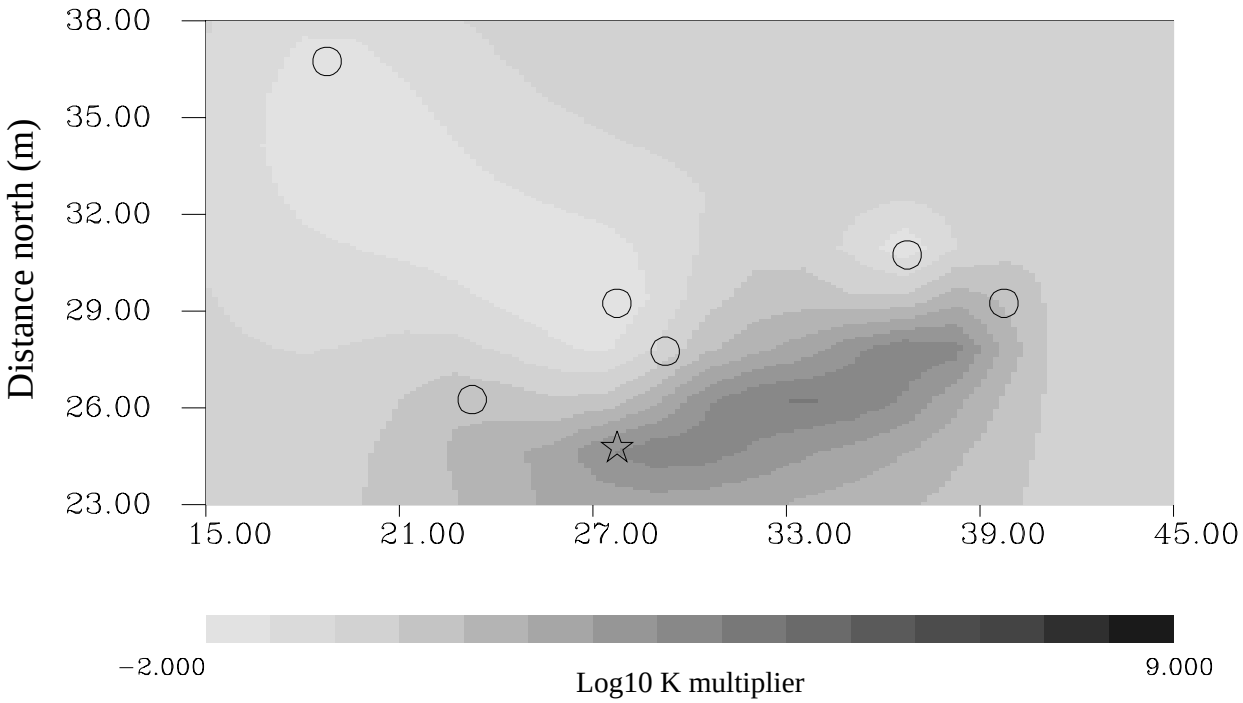
38.00
35.00
32.00
29.00
26.00
23.00
Distance north (m)
15.00
21.00
27.00
33.00
39.00
45.00
−2.000
9.000
Log10 K multiplier

Figure 14.

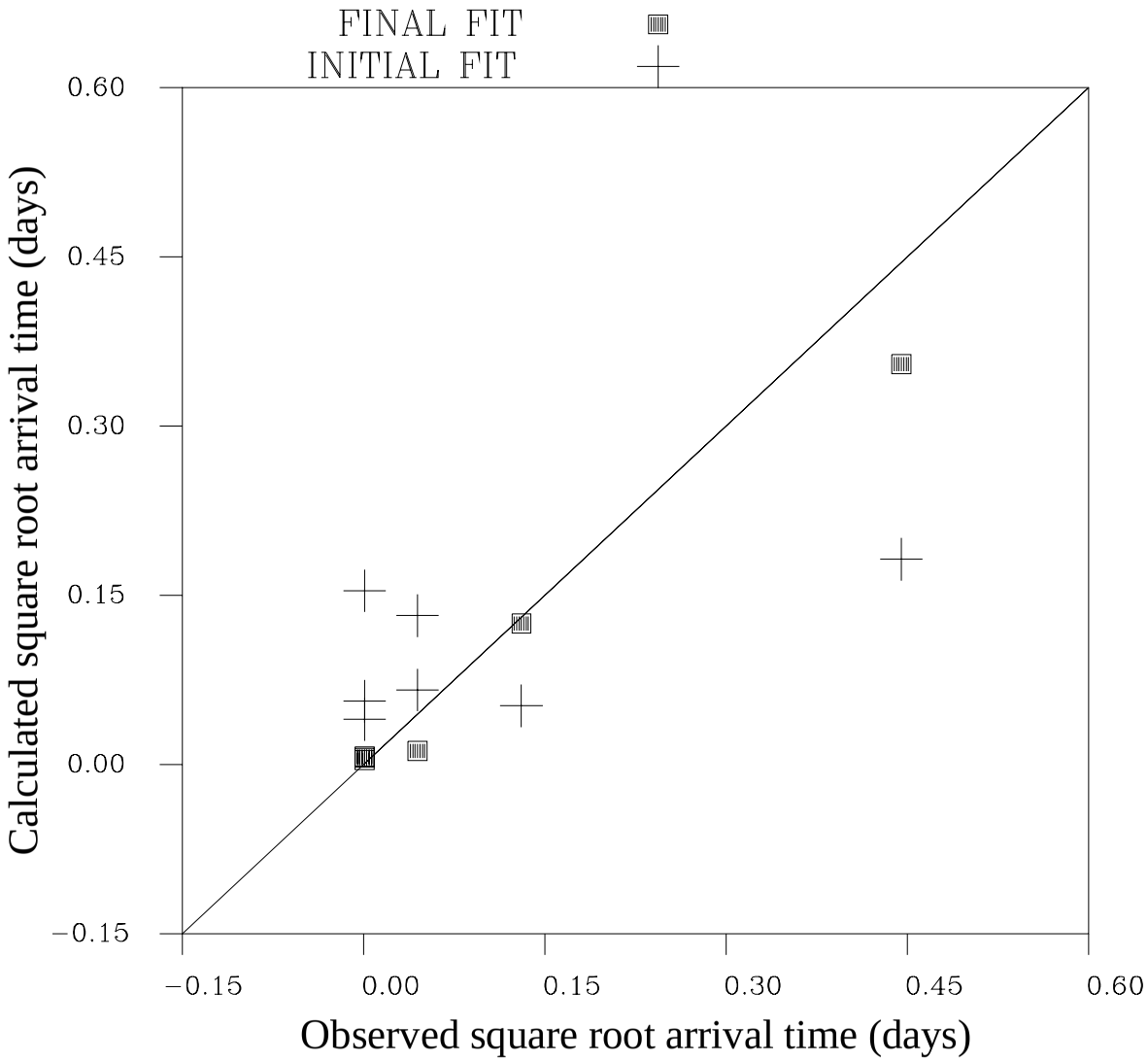
FINAL FIT
INITIAL FIT
0.60
0.45
0.30
0.15
0.00
−0.15
Calculated square root arrival time (days)
−0.15
0.00
0.15
0.30
0.45
0.60
Observed square root arrival time (days)

Figure 15.

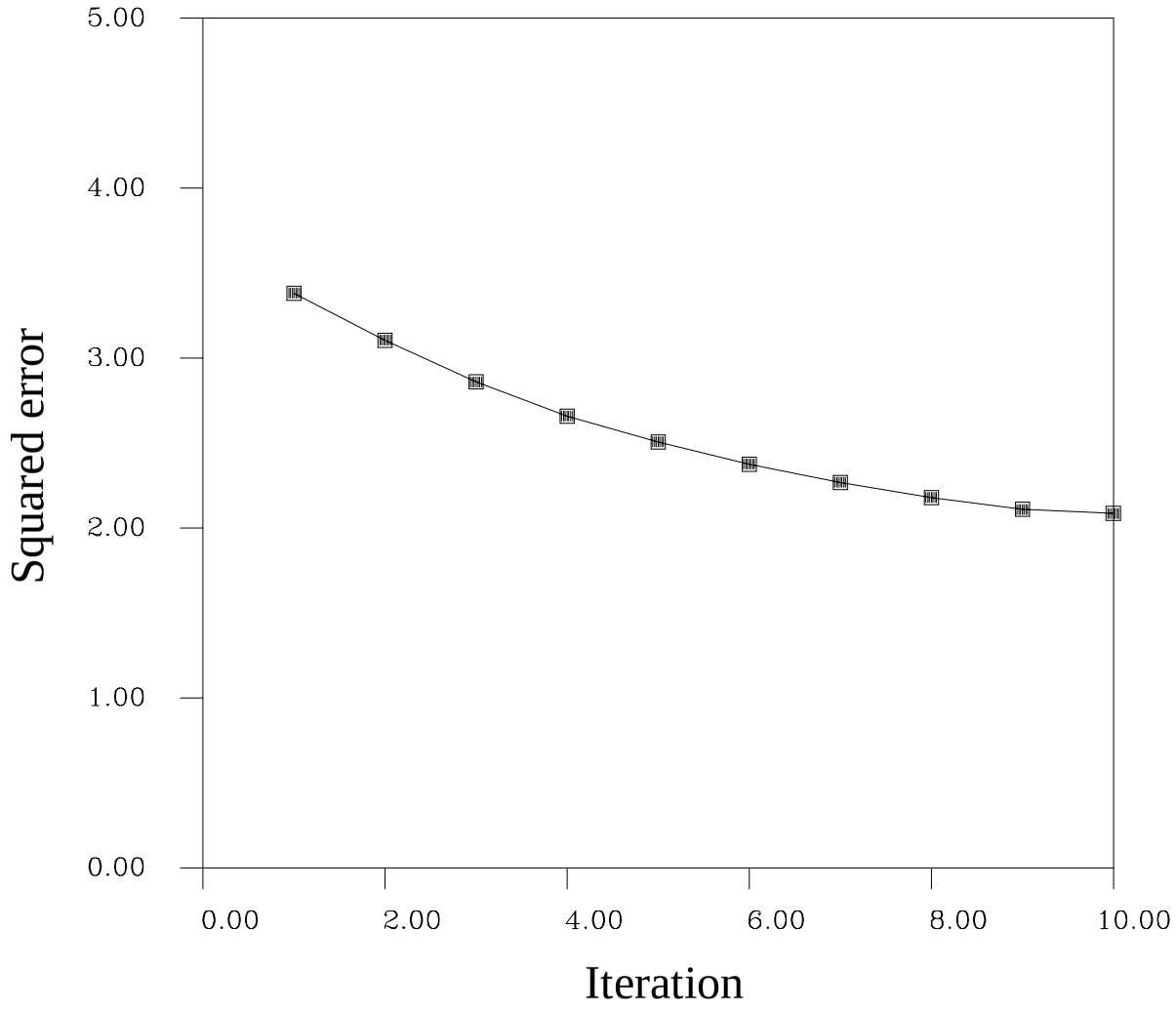
5.00
4.00
3.00
2.00
1.00
0.00
Squared error
0.00
2.00
4.00
6.00
8.00
10.00
Iteration

Figure 16.

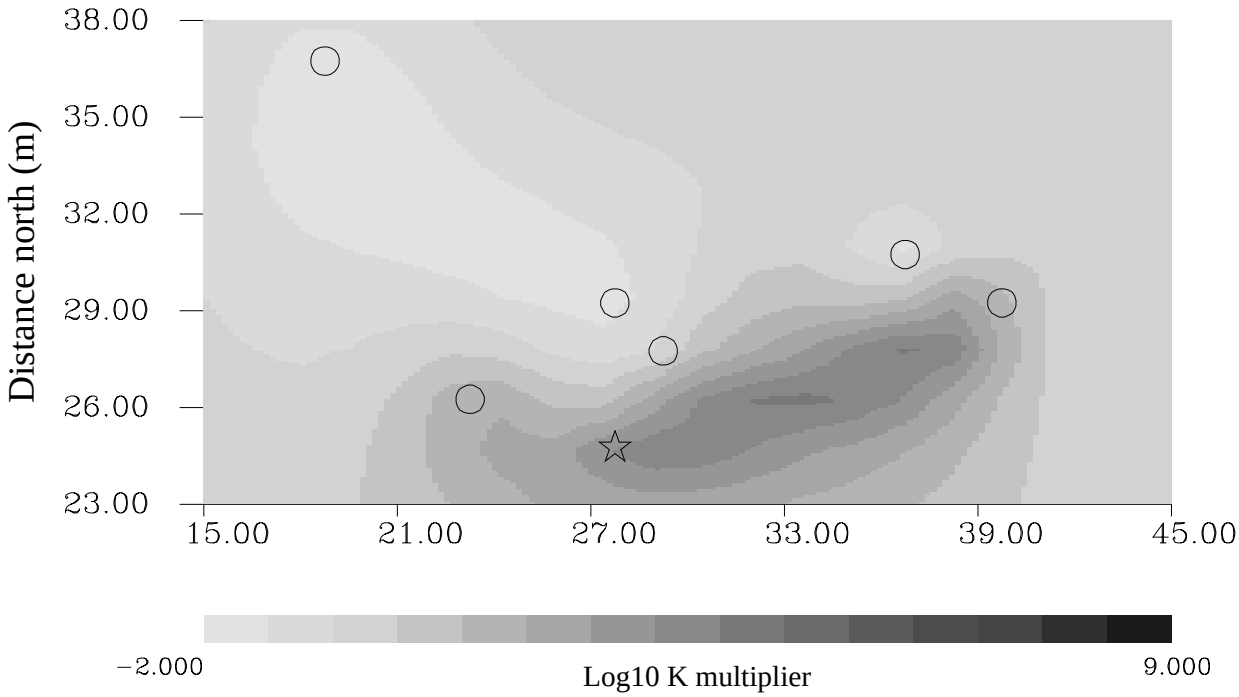
38.00
35.00
32.00
29.00
26.00
23.00
Distance north (m)
15.00
21.00
27.00
33.00
39.00
45.00
−2.000
9.000
Log10 K multiplier

Figure 17.

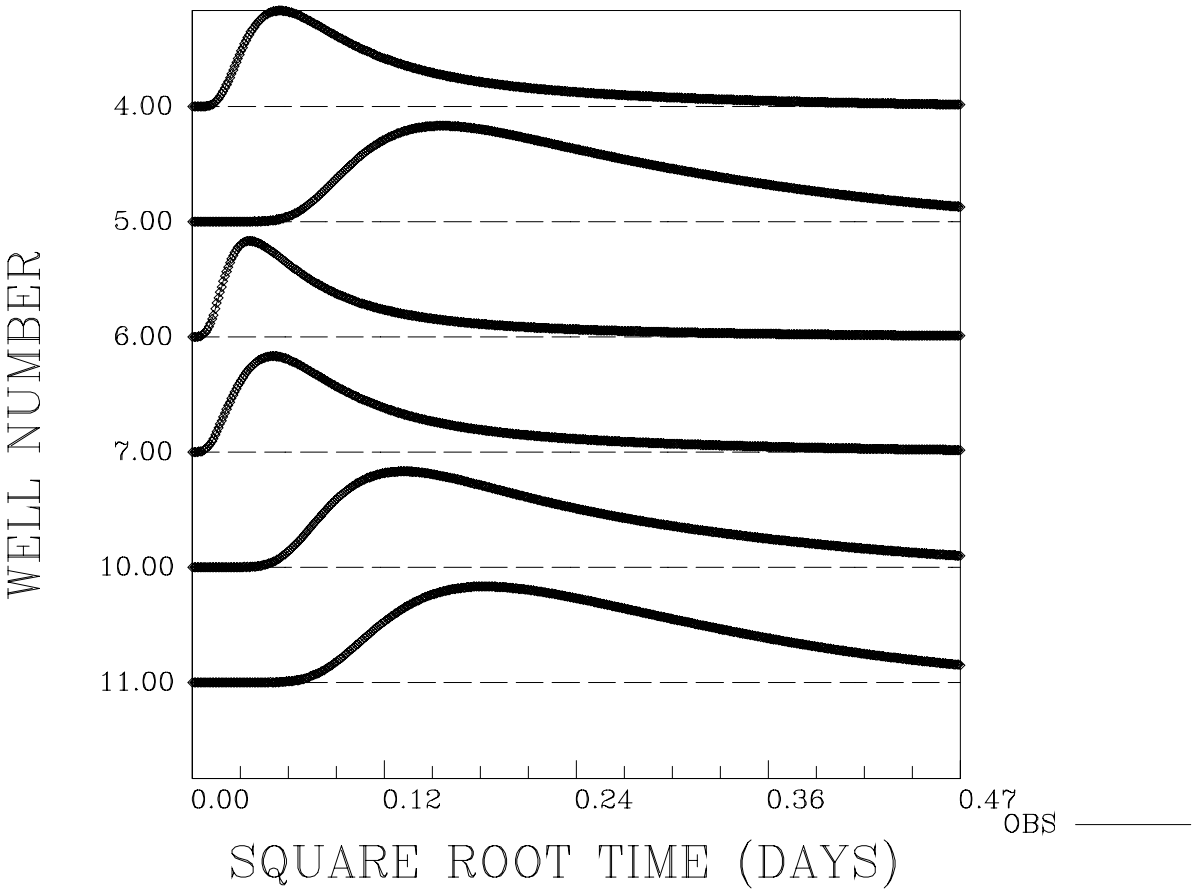
WELL NUMBER
4.00
5.00
6.00
7.00
10.00
11.00
0.00
0.12
0.24
0.36
0.47
OBS
SQUARE ROOT TIME (DAYS)

Figure 18.

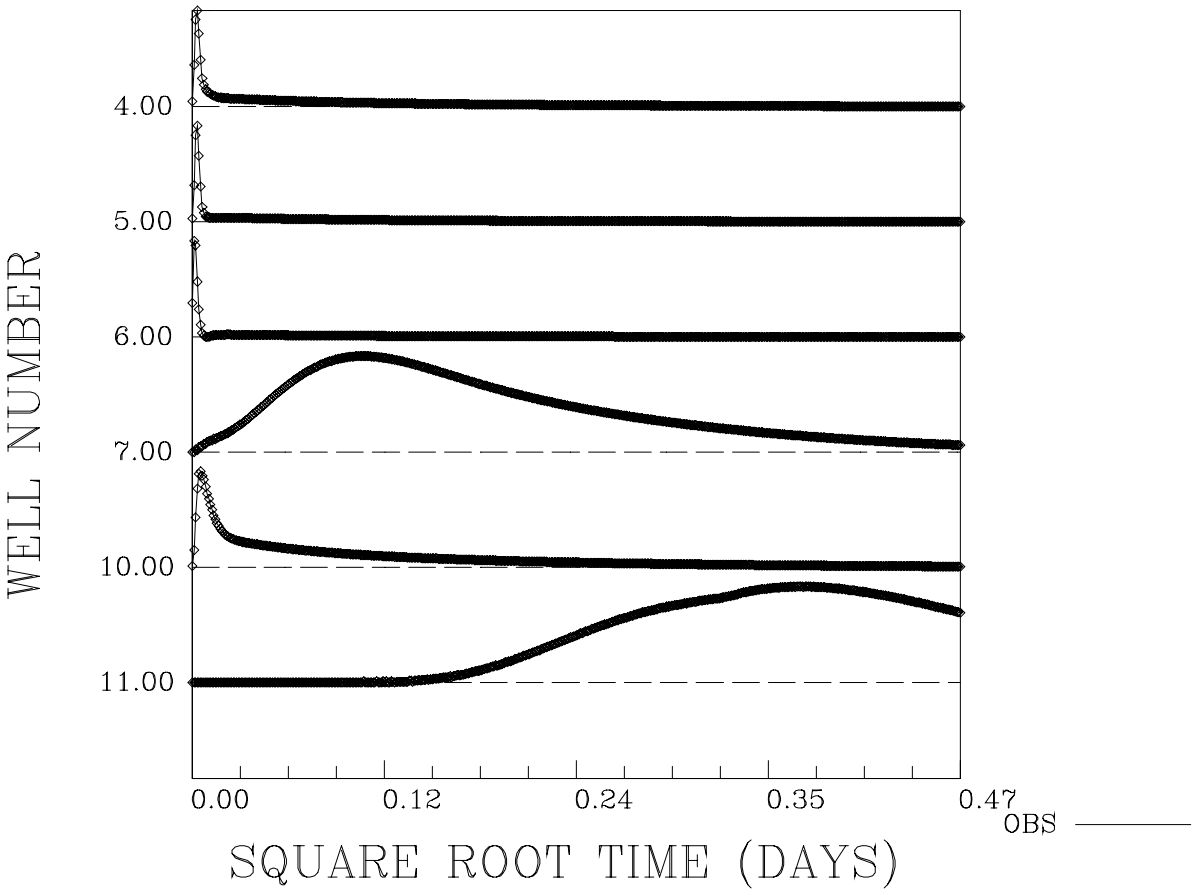
WELL NUMBER
4.00
5.00
6.00
7.00
10.00
11.00
0.00
0.12
0.24
0.35
0.47
OBS
SQUARE ROOT TIME (DAYS)

Figure 19.